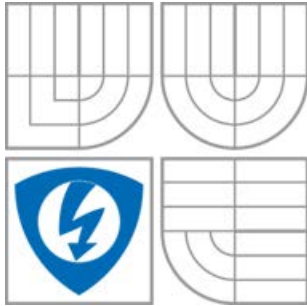


BRNO UNIVERSITY OF TECHNOLOGY



FACULTY OF ELECTRICAL ENGINEERING AND  
COMMUNICATIONS  
DEPARTMENT OF RADIO ELECTRONICS

## **LASER BEAM SHAPING**

MASTER'S THESIS

AUTHOR

Bc. CARLOS GONZÁLEZ GÓMEZ

SUPERVISOR

Ing. JURAJ POLIAK

BRNO 2012

**ESCUELA TÉCNICA SUPERIOR DE INGENIEROS  
INDUSTRIALES Y DE TELECOMUNICACIÓN**

**UNIVERSIDAD DE CANTABRIA**



***Proyecto Fin de Carrera***

**LASER BEAM SHAPING**

Para acceder al Título de

**INGENIERO DE TELECOMUNICACIÓN**

**Autor: Carlos González Gómez**

**BRNO 2012**

Brno, the 7th of June 2012

Ing. Juraj Poliak

Supervisor



**FACULTY OF ELECTRICAL ENGINEERING AND  
COMMUNICATIONS  
DEPARTMENT OF RADIO ELECTRONICS**

**MASTHER'S THESIS**

# **LASER BEAM SHAPING**

Author: Carlos González Gómez

Supervisor: Ing. Juraj Poliak, [xpolia00@stud.feec.vutbr.cz](mailto:xpolia00@stud.feec.vutbr.cz)

There are many applications of lasers which benefit from a uniform optical intensity distribution. Beam shaping is focusing on the ways how to convert input Gaussian beam into more uniform output beam. There are several methods to shaping laser beam profiles (e.g. reflective method, refractive method, diffractive method, application of diffusers). The aim of this project is to transform input Gaussian beam into output Top Hat beam. Theoretical analysis will be performed and practical transformation will be realized.

[1] DICKEY, M. F., HOLSWADE, S. C. Laser beam shaping: theory and techniques. New York: CRC Press, 2000.

[2] DICKEY, M. F., HOLSWADE, S. C., SHEALY, D. L. Laser Beam Shaping Applications. New York: CRC Press, 2005.

## **Abstract**

In this thesis, the author has tried to research about several methods and techniques to transform a Gaussian input beam of a optical system into a flat-top (uniform) output beam. In practical part, approaches of geometrical and diffusers techniques are used. The model of diffuser will be experimentally confirmed during the experiment. In the final part, results of this experiment and simulation are discussed.

## **Keywords**

Gaussian beam, flat-top beam, diffraction, refractive optical system, diffusers.

## **Resumen**

En esta tesis, el autor ha tratado de investigar varios métodos y técnicas para transformar un haz de rayos en la entrada del sistema óptico con distribución Gaussiana en un haz de rayos en salida con una distribución uniforme. En la parte práctica se usan enfoques de las técnicas geométricas y de difusores. El modelo del difusor será confirmado con un experimento. Al final los resultados del experimento y la simulación serán discutidos

## **Palabras clave**

Haz Gaussiano, haz uniforme, difracción, sistema óptico refractivo, difusores.

## Declaration

I hereby confirm that I worked out this thesis, entitled “Laser Beam Shaping”, myself with aid of my project leaders, bibliography, documentation and other sources of information that are mentioned in the end of thesis.

Brno, the 7th of June 2012

Carlos González Gómez

## Acknowledgements

I would like to mention everyone who helped me during writing this thesis.

Firstly I want to thank to my master thesis supervisor Ing. Juraj Poliak for all his motivation and help when I needed.

Secondly I must thank to all my family who are far from here. They have made possible that I could come to Brno to make my master thesis. My parents, my brother, my grandparents, my uncles, my aunts and my cousins have supported me at all times. Although the most important person for me this year have been my girlfriend. We have been all the year separated, however, she has always remembered me and has tried I have a great time here.

Finally I would like to thank to all my friends. My friends from Torrelavega and Santander who have grown with me and especially my friends from Erasmus who have shared best year of our life.

# Contents

1. INTRODUCTION .....	13
2. FIELD MAPPERS .....	14
2.1 Diffraction theory techniques.....	17
2.1.1 The analytical solution .....	17
2.1.1.1 Optical configuration.....	18
2.1.1.2 Minimum mean square error formulation.....	18
2.1.1.3 Stationary phase solution.....	20
2.1.1.4 Quadratic Phase Correction .....	22
2.1.2 Design considerations .....	23
2.1.3 Method of design .....	24
2.2 Geometrical techniques.....	29
2.2.1 Theory of laser beam profile shaping .....	29
2.2.1.1 Optical design and energy balance condition .....	32
2.2.1.2 Solution of the differential equations .....	35
2.2.2 Refractive intensity profile shaping systems .....	36
2.2.2.1 Method of design .....	38
a. Definitions.....	39
b. Choice of output beam profile .....	41
c. Propagation.....	43
d. Calculation of aspheric surfaces.....	44
2.3 Optimization techniques.....	48
2.3.1 Theory and Optimization .....	50
2.3.2 Applications.....	51
2.3.2.1 Design and Analysis of a Beam Shaper Projector.....	51

2.3.2.2	Design and Analysis of a Gradient Index Shaper.....	52
3.	Beam Integration.....	53
3.1	Beam shaping with diffractive diffusers .....	54
3.1.1	Properties of diffractive diffusers .....	54
3.1.1.1	Near field beam shapers (remapping optics).....	54
3.1.1.2	Far field shapers .....	57
3.1.1.3	Mathematical description of a diffuser.....	60
3.1.2	Design example .....	62
3.1.3	Experimental results .....	69
3.1.4	Applications of diffusers.....	73
4.	Conclusion .....	75
	References.....	76
	Appendix A .....	77
	Appendix B .....	79
	Appendix C .....	80

## List of Figures

<b>Figure 2.1</b>	General beam shaping problem .....	14
<b>Figure 2.2</b>	Shaping a Gaussian beam to a uniform beam.....	15
<b>Figure 2.3</b>	Fourier transform beam shaping system .....	18
<b>Figure 2.4</b>	System optical layout .....	24
<b>Figure 2.5</b>	Rectangular and circular phase function and 10 <sup>th</sup> order fit .....	25
<b>Figure 2.6</b>	Simulation of output beam. $\beta x = 8$ and $\beta y = 16$ . .....	28
<b>Figure 2.7</b>	Conservation of energy within a bundle of rays .....	31
<b>Figure 2.8</b>	Ray paths in a convention, refractive beam reshaping system. ....	33
<b>Figure 2.9</b>	Interference pattern produced by a four-beam holographic projection processing system when illuminated with a Gaussian beam. The image on the left side of the figure was taken near the centre of the beam, and the image on the right side of the figure was taken near the edge of the beam.....	37
<b>Figure 2.10</b>	Holographic projection system .....	37
<b>Figure 2.11</b>	Super Gaussian function for $p=2, 4, 8$ and $12$ . .....	42
<b>Figure 2.12</b>	Relationship between efficiency and peak to peak uniformity for various beam profiles. Solid curves are for Fermi Dirac functions with, from bottom to top, $\beta=5, 10$ and $15$ ; dashed curves are for super Gaussian functions with, from bottom to top, $p=2$ (Gaussian), $4, 8$ , and $16$ . .....	42
<b>Figure 2.13</b>	Effect of diffraction on Fermi Dirac beams with $R0 = 3.25 \text{ mm}$ after propagating $1 \text{ m}$ . .....	44
<b>Figure 2.14</b>	Schematic representation of a Keplerian beam reshaping system, showing the path of a typical ray.....	45
<b>Figure 3.1</b>	Typical system layout of a near field beam shaper. Only the first optic is required to shape the beam at plane $z=d$ . to extend the range at which the top hat will exist requires a second optic to correct for aberrations in the phase of the beam. ....	55
<b>Figure 3.2</b>	System to transfer the shaped beam into the far field. A simple lens with the appropriate focal length can be added after this system to re-collimate the beam. ....	56

<b>Figure 3.3</b>	Simulations result of the output intensity of a Gaussian to square super Gaussian top hat beam shaper. (a) The result with the perfect input beam. The output is >99% efficient and the peak to valley non uniformity is <2%. (b) The result with an input that is 5% too large. The peak to peak non uniformity is about 18%.....	57
<b>Figure 3.4</b>	(a) The phase of the Gaussian to square super Gaussian top hat beam shaper shown in Figure 3.3. (b) A portion of the phase of a diffuser that projects a square energy envelope-.....	58
<b>Figure 3.5</b>	The wave vector map of light as it is transmits through a periodically varying structure such as a grating. The lower portion of the plot shows the x component summations of the undeviated beam ( $K_0$ ) and the grating vector ( $K_g$ )..	60
<b>Figure 3.6</b>	A plot of the spatial frequency band that is desired in the ring diffuser design example. The plot represents a subsection of the 200 x 200 calculation grid. ...	64
<b>Figure 3.7</b>	Randomized values between 0 and 1.....	65
<b>Figure 3.8</b>	Spatial frequency band randomized real .....	66
<b>Figure 3.9</b>	Spatial frequency band randomized imaginary .....	66
<b>Figure 3.10</b>	A portion of the binary (two levels) phase structure for the ring diffuser. ....	68
<b>Figure 3.11</b>	Realization of the experiment .....	70
<b>Figure 3.12</b>	Input Beam .....	71
<b>Figure 3.13</b>	Diffuser detail .....	72
<b>Figure 3.14</b>	Output beam .....	72

## List of Tables

<b>Table 1</b>	Parameters for the circular and rectangular cross section. ....	25
<b>Table 2</b>	Values of parameters.....	26
<b>Table 3</b>	Coefficients of the sagitta function .....	27
<b>Table 4</b>	Definition of variables for the design of a diffuser.....	62
<b>Table 5</b>	Specifications of the diffuser .....	69

## 1. INTRODUCTION

Ever since the invention of the laser, it has been recognized that the typical intensity distribution of a laser beam is often undesirable for practical applications, especially those requiring uniform illumination of an extended area. The beam emitted from a high-Q optical cavity oscillating in the fundamental  $TEM_{00}$  mode has a radial intensity dependence that follows a Gaussian profile. This profile closely describes the observed output of many lasers and it also approximates the intensity distribution of the collimated output of a single mode optical fiber and the central region of the output of a single of a spatial filter. Hence one repeatedly encounters the problem of uniformly illuminating some region of interest given a Gaussian laser beam as a light source [1].

To solve this problem, we use laser beam shaping, which is the process of redistributing the irradiance and phase of a beam of optical radiation. In the first part of the thesis, field mappers methods are described. Diffraction or geometrical techniques are used to get more uniform beams in the output of the optical system.

In the second part beam integration techniques as diffusers are developed to achieve our desirable output. The thesis concludes with a simulation of real beam and experimental verification of this program.

## 2. FIELD MAPPERS

We can see the general beam shaping problem in Figure 2.1 [2]. A beam is incident upon an optical system that may consist of one or more elements. The optical system must operate upon the beam to produce the desired output. The desired output might only demand a certain irradiance distribution at a target plane, with the phase allowed to vary. This would be the entire problem for the case of incoherent beams. For coherent beams, the designer may or may not want to constrain the phase of the beam at the output plane. For example, if a collimated output beam is desired, the phase front of the beam exiting the optical system must be uniform. If the design only requires a certain irradiance distribution at the target, however, the optical system is usually simpler if the phase is left unconstrained.

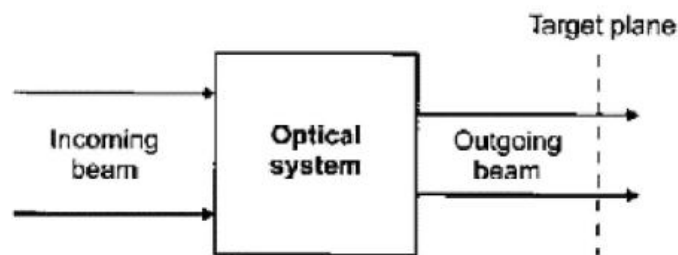


Figure 2.1 General beam shaping problem

The essence of the beam shaping problem is illustrated in Figure 2.2 in which an input beam of rays, in this case with Gaussian distribution, is incident on a plane representing the optical system [2]. The output rays are bent so as to come to a uniform distribution in the output plane. This is the Gaussian to flat-top beam shaping problem. A wavefront can be computed by noting that in the geometrical optics approximation rays are normal to the wavefront. Once the wavefront is determined one can then determine a phase function that would produce the shaped beam. Implementing the phase function may be a complicated optical design process, and may be best achieved with multiple optical surfaces (element).

Determining the optical phase element is a complicated problem. Complications arise if the thin element approximation is not applicable, or if both phase and irradiance profiles are specified.

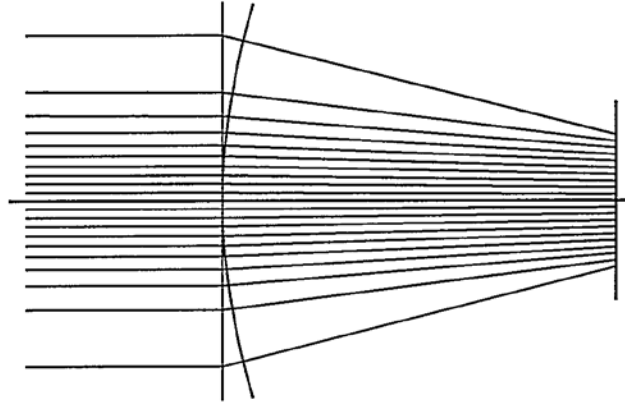


Figure 2.2 Shaping a Gaussian beam to a uniform beam

In addition to the above, what can be obtained for a given beam shaping problem is limited by physical optics (electromagnetic theory). The simplest result of this theory is an uncertainty principle that depends upon input beam size and wavelength, and output profile size and distance. This result is closely related to diffraction limits on imaging optical systems.

Only lossless or low-loss shaping techniques are considered. If large losses are allowed the beam shaping problem becomes trivial. For most applications, efficiency requirements generally mandate low-loss systems. Low-loss beam shaping for laser sources can be broken down into two basic categories. The first, field mapping, includes methods where the input profile is redistributed at the target plane, such as the ray bending scheme in Figure 2.2.

Field mappers work only for beams with a known field distribution, such as single-mode beams, and they are generally highly sensitive to alignment and beam dimensions.

Like many optical problems, there is no single beam shaping method that addresses all situations. The nature of the input beam, the system geometry, and

the quality of the desired output beam all affect the choice of technique. In considering a beam shaping application for single-mode Gaussian beams, it is first advisable to calculate the parameter

$$\beta = \frac{2\sqrt{2\pi}r_0y_0}{f\lambda}$$

where  $\lambda$  is the wavelength,  $r_0$  is the radius at the  $1/e^2$  point of the input beam,  $y_0$  is half-width of the desired output dimension, and  $f$  is the focal length of the focusing optic, or the working distance from the optical system to the target plane for systems without a defined focusing optic.

## **2.1 Diffraction theory techniques**

This design is based on a Fourier transform relation between the input and output beam functions. The diffraction approach introduces a parameter that contains the product of the widths of the input and output beams. The quality of the solution improves asymptotically with increasing value of the parameter.

For single-mode beams with Gaussian profile it is possible to map the beam into a uniform intensity profile with steep skirts. This mapping can be accomplished with simpler, optics that is more flexible with respect to scaling and does not have the interference patterns inherent in multi-faceted beam integration.

The configuration analyzed exploits the Fourier transform properties of lenses. Like we have already said, the output optical field is the Fourier transform of the input optical field and a phase function. This configuration has the advantage of being able to change the output size or the working distance by changing the transform lens.

### **2.1.1 The analytical solution**

In the Figure 2.1 we can see that the beam to be shaped enters the proverbial black box from the left and exits on the right, diffracting to the design irradiance pattern. The black box may contain a single optical element or a combination of several optical components of differing types such as lenses, mirrors, prisms, diffractive optics and holograms.

### 2.1.1.1 Optical configuration

Our approach to lossless beam shaping consists of a phase element in conjunction with a Fourier transform lens like we can see in Figure 2.3. The optical field at the focal plane of the transform lens is proportional to the Fourier transform of the product of the input optical field and phase of the phase element. The phase element can be changed to control both the scale and shape of the output irradiance. The transform lens can be changed to modify the working distance, with a corresponding change in scale of the output.

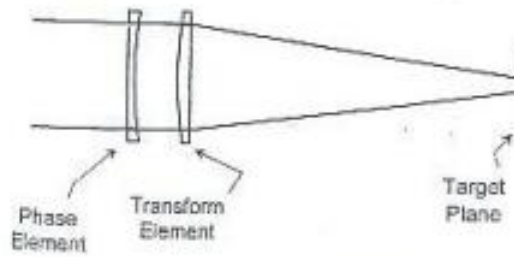


Figure 2.3 Fourier transform beam shaping system

### 2.1.1.2 Minimum mean square error formulation

The problem is to design the phase element. The direct approach would be to solve for the phase element that minimizes the mean square difference between the desired irradiance and the irradiance produced by the phase element. We want to find  $\phi$  that minimizes an integral of the form

$$R = \int \left| \left| \mathcal{F} \left[ (2/\sqrt{\pi})^{1/2} e^{-x^2} e^{i\phi} \right] \right|^2 - (1/\alpha)^{1/2} \text{rect}(f/\alpha) \right|^2 df \quad (2.1)$$

where  $\mathcal{F}$  denotes a Fourier transform operation,  $f$  denotes the corresponding frequency domain variable,  $\alpha$  defines the size of the output, and the problem is scaled to a unit width ( $1/e^2$ ) Gaussian beam function. Here, the problem is formulated in one dimension, which is appropriate to the separable problem of

converting a circular Gaussian beam into a uniform beam with a square cross section.

The solution to the separable uniform amplitude and phase problem can be obtained by determining the phase  $\phi$  that minimizes the functional

$$\begin{aligned}
 R &= \int \left| \mathcal{F} \left[ \left( \frac{2}{\sqrt{\pi}} \right)^{\frac{1}{2}} e^{-x^2} e^{i\phi} \right] - \left( \frac{1}{\alpha} \right)^{\frac{1}{2}} \text{rect} \left( \frac{f}{\alpha} \right) \right|^2 df \\
 &= 2 - 2\text{Re} \int \mathcal{F} \left[ \left( \frac{2}{\sqrt{\pi}} \right)^{\frac{1}{2}} e^{-x^2} e^{i\phi} \right] \left( \frac{1}{\alpha} \right)^{\frac{1}{2}} \text{rect} \left( \frac{f}{\alpha} \right) df \quad (2.2)
 \end{aligned}$$

This equation differs from that of equation (2.1) in that it involves the differences of fields (complex) function, while equation (2.1) is the difference of intensities (magnitude squared) functions. Thus, the problem described in equation (2.1) is less constrained since the phase of the output is a free parameter. This allows for a broader range of solutions. In equation (2.2) the input Gaussian function and the output rect function are normalized to unit energy. This insures that the mean square difference in equation (2.2) depends on the variation in the shape of the input and output functions and not on any relative amplitude difference between the two functions.

The solution to equation (2.2) is readily obtained by applying Parseval's theorem and expanding the integrand.

$$R = 2 - 2\text{Re} \int \left( \frac{2\alpha}{\sqrt{\pi}} \right)^{\frac{1}{2}} e^{-i\phi} \text{sinc}(\alpha x) e^{-x^2} dx \quad (2.3)$$

Here,  $\text{Re } z$  denotes the real part of  $z$ . Clearly,  $R$  is minimized if the integral is maximized. This is obtained if  $\phi$  is set equal to the phase of the sinc function. Since the phase of the sinc function is a binary function with values of 0 and  $\pi$ , the optimum phase function is a binary function.

### 2.1.1.3 Stationary phase solution

Solutions to the problem defined by the equation (2.1) can be obtained by application of the method of stationary phase. This method gives us an asymptotic approximation to integrals of the form

$$I(\beta) = \int_a^b f(x)e^{i\beta\phi(x)} dx \quad (2.4)$$

where  $\beta$  is a dimensionless parameter. The first term in the asymptotic phase approximation to the integral is given by

$$I_c(\beta) \sim e^{i\{\beta\phi(c) + \frac{\mu\pi}{4}\}} f(c) \left[ \frac{2\pi}{\beta|\phi''(c)|} \right]^{\frac{1}{2}} \quad (2.5)$$

where primes denote derivatives,

$$\mu = \text{sign}\phi''(c) \quad (2.6)$$

and  $c$  is a simple stationary point defined by

$$\phi'(c) = 0, \quad \phi''(c) \neq 0 \quad (2.7)$$

The essence of the beam shaping problem is to equate  $|I_c(\beta)|^2$  with the desired irradiance in the output plane. Using this condition with equation (2.7) leads to a second order differential equation for the beam shaping phase function  $\phi(x)$ . Care must be taken with respect to the absolute value of  $\phi''$  in the denominator of equation (2.5). This condition requires that the phase  $\phi(x)$  is a convex function whose second derivate is either positive or negative everywhere. This turns out not to be a problem for the case of mapping a Gaussian into a rect function. This can be seen from the geometrical optics representation of the beam shaping illustrated in the Figure 2.2 where the input beam consists of collimated rays whose density is accurately scaled to be proportional to a Gaussian irradiance profile. These rays are bent, in the shaping plane, to form a uniform irradiance distribution in the output plane. Near the shaping plane one can form a phase front for the converging beam by integrating the reciprocal of the slope of the rays (wave normal). The curved line

in the figure represents the phase front. It can be seen that the slope of the phase front, derivative of the phase function, is a monotonic function giving a phase function with a positive (or negative) second derivative.

In two dimensions, the general form of the equation to be solved is

$$F(\omega_x, \omega_y) = \frac{1}{2\pi} \int_{-\infty}^{\infty} \int_{-\infty}^{\infty} f(\xi, \eta) \exp(i(\beta\phi(\xi, \eta) - \xi\omega_x - \eta\omega_y)) d\xi d\eta \quad (2.8)$$

where  $\xi = x/r_i$  and  $\eta = y/r_i$  are normalized input variables with  $r_i$  defining the length scale, and  $w_{x=x_f}/r_0$  and  $w_{y=y_f}/r_0$  are normalized output variables in the focal plane of the Fourier transform lens with  $r_0$  defining the length scale. The stationary phase solution improves asymptotically with increasing dimensionless parameter  $\beta = 2\pi r_i R_0 / f\lambda$  where  $R_0$  is the size of the output beam,  $\lambda$  is the optical wavelength and  $f$  is the focal length of the transform lens.

The stationary phase evaluation of equation (2.8) allows for the mapping of arbitrary single mode laser beams into arbitrary irradiance profiles. We can obtain solutions for the problem of converting circular Gaussian beams to uniform profiles with rectangular cross sections and the problem of converting circular Gaussian beams to uniform beams with circular cross-sections.

For a circular Gaussian beam input, the problem of turning a Gaussian into a flat-top beam with rectangular cross section is separable. This is, the solution is the product of two one-dimensional solutions.  $\beta$  and  $\phi(\xi)$  are thus calculated for each dimension. The phase element will then produce the sum of these phases ( $\beta_x\phi_x(x) + \beta_y\phi_y(y)$ ). The corresponding one dimension solution for  $\phi$  is

$$\phi(\xi) = \frac{\sqrt{\pi}}{2} \xi \operatorname{erf}(\xi) + \frac{1}{2} \exp(-\xi^2) - \frac{1}{2} \quad (2.9)$$

where

$$\xi = \frac{\sqrt{2}x}{r_0} \quad \text{or} \quad \xi = \frac{\sqrt{2}y}{r_0}$$

and  $r_0 = 1/e^2$  radius of the incoming Gaussian beam.

The solution for the problem of turning a circular Gaussian beam into a flat-top beam with circular cross-section is

$$\phi(\xi) = \frac{\sqrt{\pi}}{2} \int_0^\xi \sqrt{1 - \exp(-\rho^2)} d\rho \quad (2.10)$$

where

$$\xi = \frac{\sqrt{2}r}{r_0}$$

and  $r = \text{radial distance}$  from the optical axis.

The quality of these solutions depend strongly on the parameter  $\beta$ , given by

$$\beta = \frac{2\sqrt{2\pi}r_0y_0}{f\lambda} \quad (2.11)$$

#### 2.1.1.4 Quadratic Phase Correction

The solutions previously described assume that the input Gaussian beam has a uniform (constant) phase at the beam shaping element. For a Gaussian beam this condition is obtained at the beam waist, and it is not convenient or practical to always locate the beam waist at the shaping element. A practicable solution is to exploit the fact that the Gaussian beam phase causes a shift in the location of the output plane. That is, the desired profile is located a distance from the focal plane of the transform lens.

Gaussian beams propagate with a phase function given by

$$f(x, y) = e^{(-\sigma + i\gamma)(x^2 + y^2)} \quad (2.12)$$

where  $\sigma$  and  $\gamma$  are functions of the distance from the beam waist, and  $\gamma = 0$  at the beam waist. The solutions to the above problem assume that  $\gamma = 0$  and the output is the Fourier transform of the product of a Gaussian and the beam shaping phase function given by

$$U(x_f, y_f) = A e^{i\left(\frac{k}{2f}\right)(x_f^2 + y_f^2)} \iint e^{-\sigma(x^2 + y^2)} e^{i\beta\phi} e^{i(2\pi/\lambda f)(xx_f + yy_f)} dx dy \quad (2.13)$$

where  $x, y$  are the input coordinates and  $x_f, y_f$  are the output coordinates in the focal plane of the transform lens.

### 2.1.2 Design considerations

A primary design advantage of this lossless beams shaping technique is that the designer can start with a desired target spot quality and determine the optical system required. This is because the dimensionless quantity  $\beta$  of equation (2.11) completely determines the quality of the spot at the target plane. Different optical configurations and wavelengths will produce the same target spot quality if they share the same value of  $\beta$ . Low values of  $\beta$  produce target spots with more rounded sides and wider skirt regions, while higher values of  $\beta$  more closely approach the geometric ideal of a uniform intensity profile with infinitely steep sides. The cost of increasing  $\beta$  involves either increasing the size of the Gaussian beam at the phase element or reducing the wavelength. The designer can determine the minimum  $\beta$  that will satisfy the needs, and design the most economical system.

Figure 2.4 shows a standard layout for a beam shaping optical system [2]. For most design situations, the size of the target spot and the wavelength will be determined by the application. The focal length of the transform lens may also be determined by standoff or other considerations, although a minimum focal length will maximize  $\beta$ . The final variable is the Gaussian beam radius at the shaping element. To achieve the desired  $\beta$ , the beam size should be expanded by an afocal telescope, as shown in the figure. With the optical system designed for one target geometry, there are two methods to produce additional target geometries. The first is to change the phase element. With the same expansion and focusing optics, a system could thus produce circular and rectangular beams of several sizes. However, that different target geometries will vary  $\beta$ , and hence spot quality, as determined by equation (2.11). The second method involves changing the focusing, or transform, lens while leaving the

telescope and the phase element fixed. This change can vary only the target size, not the geometry, but it has the advantage of maintaining a constant target spot quality. The variation in the focal length changes the spot size proportionally, and thus  $\beta$  remains constant.

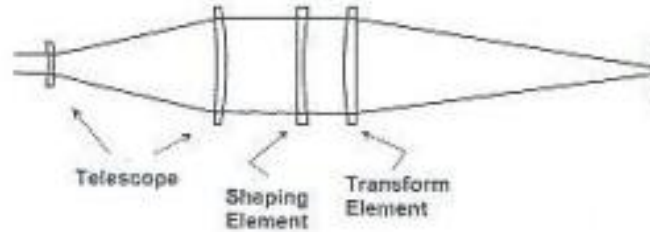


Figure 2.4 System optical layout

Once a target spot quality is determined, the required phase profile imparted on the beam by the phase element is then found by multiplying the phase function of equations (10) or (11) by  $\beta$ . This multiplication scales the phase function to the particular geometry of the application. A telescope is then designed to expand the beam to the required value. A transform lens of the required focal length completes the system.

### 2.1.3 Method of design

If we speak about the method of design, we already know that the quality of the target spot can be selected to suit the application, and the necessary optical system parameters. The size of the Gaussian beam at the phase element will be the free variable that determines  $\beta$ . If the phase element and the optical system are to be studied with an optical design program, the phase function will need to be expressed as a polynomial. In order to facilitate modeling, the phase functions for rectangular and circular spots have been fitted to 10<sup>th</sup>-order polynomials. The fits are good to  $\xi = 3\sqrt{2}$ , which is  $3r_0$  at the phase element. The form of rectangular and circular cross section is

$$\phi(\xi) = a_2\xi^2 + a_4\xi^4 + a_6\xi^6 + a_8\xi^8 + a_{10}\xi^{10} \quad (2.14)$$

where

Rectangular spot	Circular spot
$a_2 = 4.74 \times 10^{-1}$	$a_2 = 4.31 \times 10^{-1}$
$a_4 = -5.5 \times 10^{-2}$	$a_4 = -4.37 \times 10^{-2}$
$a_6 = 4.99 \times 10^{-3}$	$a_6 = 3.65 \times 10^{-3}$
$a_8 = -2.37 \times 10^{-4}$	$a_8 = -1.65 \times 10^{-4}$
$a_{10} = 4.41 \times 10^{-6}$	$a_{10} = 2.97 \times 10^{-6}$

Table 1 Parameters for the circular and rectangular cross section.

```
xi=-(3*sqrt(2)):0.01:3*sqrt(2);
N=length(xi);
for i=1:N

phi_1=a(1,1)*xi(i)^2+a(2,1)*xi(i)^4+a(3,1)*xi(i)^6+a(4,1)*xi(i)^8+a(5,1)*xi(i)^10;
    phi1(i)=phi_1;

phi_2=a(1,2)*xi(i)^2+a(2,2)*xi(i)^4+a(3,2)*xi(i)^6+a(4,2)*xi(i)^8+a(5,2)*xi(i)^10;
    phi2(i)=phi_2;
end
plot(xi,phi1,'g',xi,phi2,'r')
```

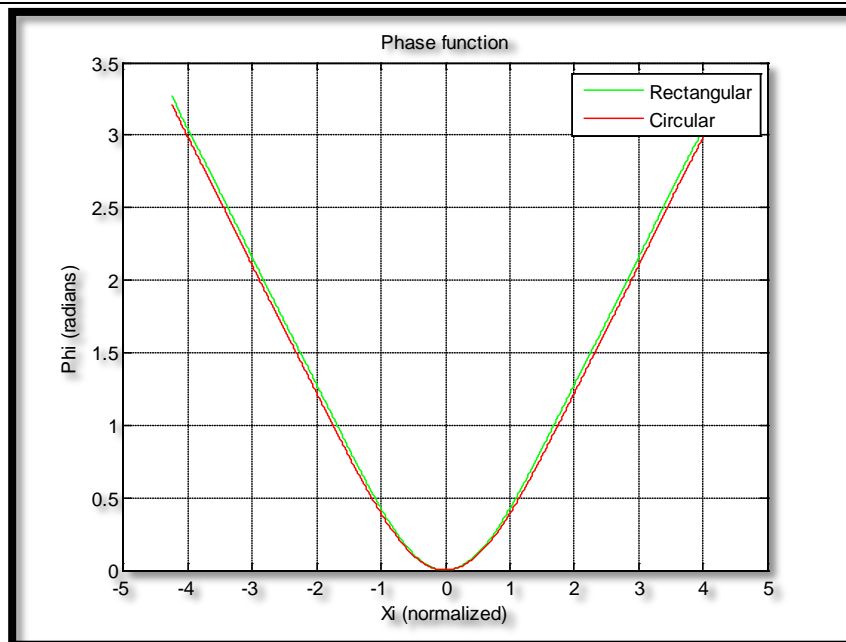


Figure 2.5 Rectangular and circular phase function and 10<sup>th</sup> order fit

Figure 2.5 show the quality of fit to the original function. The r.m.s variation between the two curves is 0.0025 radians.  $\xi$  is a radial coordinate in this case, and the phase function is radially symmetric.

To solve the problem we consider the case where a rectangular spot is desired with the next features:

<b><i>focal distance (f)</i></b>	<b>400 mm</b>
<b><i>target spot dimensions</i></b>	<b>2 mm (x axis) by 4 mm (yaxis)</b>
<b><i>laser</i></b>	<b>10.6 <math>\mu</math>m</b>
<b><i>half width of desired spot size (y<sub>0</sub>)</i></b>	<b>1 mm</b>
<b><i>n(ZnSe)</i></b>	<b>2.403</b>
<b><i>wavelength (<math>\lambda</math>)</i></b>	<b>10.6e – 3 mm</b>
<b><i><math>\beta_x</math></i></b>	<b>8</b>
<b><i><math>\beta_y</math></i></b>	<b>16</b>

Table 2 Values of parameters.

We need to develop a polynomial that yield the phase element sagitta, or deviations from a plane at the surface vertex and the surface, as a function of distances from the optic axis. The following equation gives the sagitta of the phase surface:

$$Sag(x, y) = m_2x^2 + n_2y^2 + m_4x^4 + n_4y^4 + m_6x^6 + n_6y^6 + m_8x^8 + n_8y^8 + m_{10}x^{10} + n_{10}y^{10}$$

where

$$m_i = \frac{a_i \lambda \beta_x \left(\frac{\sqrt{2}}{r_0}\right)^i}{2\pi(n-1)} \text{ and } n_i = \frac{a_i \lambda \beta_y \left(\frac{\sqrt{2}}{r_0}\right)^i}{2\pi(n-1)}$$

The coefficients in this polynomial would be

$m_2 = 1.994 \times 10^{-4}$	$n_2 = 3.988 \times 10^{-4}$
$m_4 = -1.0127 \times 10^{-6}$	$n_4 = -2.0255 \times 10^{-6}$
$m_6 = 4.0235 \times 10^{-9}$	$n_6 = 8.0471 \times 10^{-9}$
$m_8 = -8.3652 \times 10^{-12}$	$n_8 = -1.673 \times 10^{-11}$
$m_{10} = 6.8144 \times 10^{-15}$	$n_{10} = 1.3629 \times 10^{-14}$

Table 3 Coefficients of the sagitta function

If we choose to build an element with a positive phase function, the sign convention on the sagitta would be such that the phase surface had a concave shape. A simulation of the output spot from this example problem appears in Figure 2.6.

```
x=[-2:0.01:2]; %% millimeters
y=[-4:0.02:4]; %% millimeters
r0_x=(beta_x*f*lambda)/(2*sqrt(2*pi)*y0);
r0_y=(beta_y*f*lambda)/(2*sqrt(2*pi)*y0);
t=1;
for j=2:2:10
    m(t)=((a(t,1)*lambda*beta_x)*(sqrt(2)/r0_x)^j)/(2*pi*(n1-1));
    n(t)=((a(t,1)*lambda*beta_y)*(sqrt(2)/r0_y)^j)/(2*pi*(n1-1));
    t=t+1;
end
for k=1:L
    for p=1:L
        sagitta(k,p)=-
(m(1)*x(k)^2+n(1)*y(p)^2+m(2)*x(k)^4+n(1)*y(p)^4+m(3)*x(k)^6+n(3)
)*y(p)^6+m(4)*x(k)^8+n(4)*y(p)^8+m(5)*x(k)^10+n(5)*y(p)^10);
    end
end
mesh(x,y,sagitta), colorbar
```

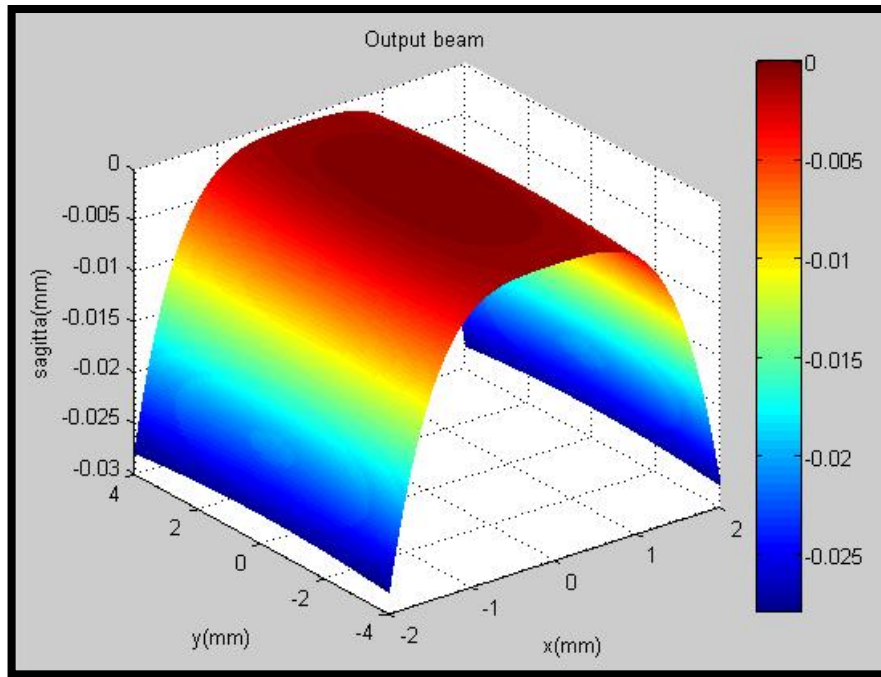


Figure 2.6 Simulation of output beam.  $\beta_x = 8$  and  $\beta_y = 16$ .

## 2.2 Geometrical techniques

Using geometrical methods to shape a laser beam profile involves application of geometrical optics to solve the optical design problem. The laws of reflection and refraction are used along with ray tracing, conservation of energy within a bundle of rays, and the constant optical path length condition to design laser beam profile shaping optical systems.

### 2.2.1 Theory of laser beam profile shaping

The concept of rays, wavefront, and energy propagation are fundamental to understanding and using geometrical optics for shaping laser beam profiles. Geometrical optics is used to set up several constraint equations which are used to determine the reflective or refractive surface shape or gradient index profile as part of the optical design of laser beam profile shaping optical systems. In order to determine or optimize the illumination within an optical system, the optical field must be determined throughout the system. The optical field is a local plane wave solution of Maxwell's equations for an isotropic, non-conducting, charge-free medium and is a solution of the scalar wave equation

$$(\nabla^2 + n^2 k_0^2)u(\mathbf{r}) = 0 \quad (2.15)$$

where  $u(\mathbf{r})$  represents the components of the electric field at the point  $\mathbf{r}$ ,  $n$  is the index of refraction at  $\mathbf{r}$ ,  $k_0 = w/c = 2\pi/\lambda_0$  is the wave number in free space,  $w$  is the frequency of the wave,  $c$  is the speed of light, and  $\lambda_0$  is the wavelength of light, so

$$u(\mathbf{r}) = u_0(\mathbf{r})\exp[ik_0 S(\mathbf{r})] \quad (2.16)$$

where  $u_0(\mathbf{r})$  and  $S(\mathbf{r})$  are unknown functions of  $\mathbf{r}$ . Equation (2.15) leads to the following conditions which must be satisfied by  $u_0(\mathbf{r})$  and  $S(\mathbf{r})$ :

$$(\nabla S)^2 = n^2 \quad (2.17)$$

$$2u_0 \nabla S \cdot \nabla u_0 + u_0^2 \nabla^2 S = 0 \quad (2.18)$$

where the term proportional to  $(1/k_0^2)$  has been neglected. Equation (2.17) is a basic equation of geometrical optics. The surfaces

$$S(x, y, z) = \text{const.} \quad (2.19)$$

are constant phase fronts of the optical field and are known as the geometrical wavefront.

Equation (2.18) is equivalent to conservation of radiant energy within a bundle of rays and leads to the geometrical optics intensity law for propagation of a bundle of rays. Using the vector identity

$$\nabla \cdot (f \cdot v) = f \nabla \cdot v + v \cdot \nabla f \quad (2.20)$$

equation (2.18) can be rewritten as

$$\nabla \cdot (u_0^2 \nabla S) = \nabla \cdot (u_0^2 n a) = 0 \quad (2.21)$$

Recognizing that energy density of a field is proportional to the square of the field amplitude  $u_0^2$  and that intensity  $I$  is equal to energy density of the field times the speed of propagation within medium, then

$$\nabla \cdot (I a) = 0 \quad (2.22)$$

Equation (2.22) expresses conservation of radiant energy for non-conducting medium. Integrating equation (2.22) over a tube surrounding a bundle of rays as illustrated in Figure 2.7 gives, after application of Gauss' theorem,

$$I_1 dA_1 = I_2 dA_2 \quad (2.23)$$

Equation (2.23) expresses conservation of energy along a ray bundle between any two surfaces intersecting the beam and is a basic equation used to design laser beam profile shaping optical system.

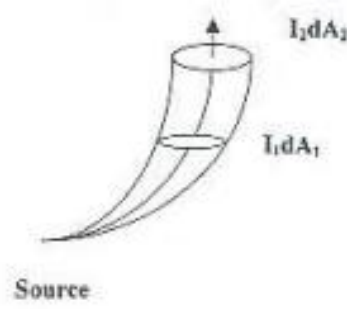


Figure 2.7 Conservation of energy within a bundle of rays

The phase and amplitude of the optical field are evaluated independently. First, the ray paths are evaluated throughout the optical system. Next, the amplitude of the optical field is determined by monitoring the intensity variations along each ray.

Rays generally characterize the direction of the flow or propagation of radiant energy, except near foci or the edge of a shadow where interference and diffraction takes place. Thus, a ray is a mathematical construct rather than a physical entity. Snell's law relates the direction of incident and refracted rays at the interface between media of different indices of refraction, which can be written in vector:

$$n(\mathbf{a} \times \hat{\mathbf{n}}) = n'(\mathbf{A} \times \hat{\mathbf{n}}) \quad (2.24)$$

where  $\mathbf{a}$  and  $\mathbf{A}$  are unit vectors along the incident and refracted rays,  $\hat{\mathbf{n}}$  is a unit vector along the normal to the interface surface with the general orientation of the incident ray, and  $(n, n')$  are the indices of refraction of the incident and refracting media. For ray tracing it is convenient to vector multiply equation (2.24) by  $\hat{\mathbf{n}}$  and simplify the resulting triple vector product into the form

$$n' \mathbf{A} = n \mathbf{a} + [n' \cos i' - n \cos i] \hat{\mathbf{n}} \quad (2.25)$$

where

$$\cos i' = \mathbf{A} \cdot \hat{\mathbf{n}} \text{ and } \cos i = \mathbf{a} \cdot \hat{\mathbf{n}} \quad (2.26)$$

and  $(i, i')$  are the angles of incidence and refraction. When mirrors are involved, the refraction ray equations can be used for reflection by setting  $n' = -n$  and using the optics sign convention. Explicitly, a unit vector  $\mathbf{A}$  along a reflected ray is given by

$$A = a - 2\hat{n}(a \cdot \hat{n}) \quad (2.27)$$

where  $\hat{n}$  is a unit normal vector at the point of reflections, and  $\mathbf{a}$  is a unit vector along the incident ray.

Each ray generally follows the path of shortest time through the optical system according to Fermat's principle which states that a ray from points  $\mathbf{P}$  to  $\mathbf{Q}$  is the curve  $\mathbf{C}$  connecting these two points that the integral

$$\text{Optical path length, } OPL(C) = \int_C n(x, y, z) ds \quad (2.28)$$

is an extreme. The quantity  $n(x, y, z)$  is the index of refraction of the medium, and  $ds$  is the infinitesimal arc length of the curve. In general, the optical path length divided by the speed of light in free space,  $c$ , gives the time for light to travel from point  $\mathbf{P}$  to  $\mathbf{Q}$  along the ray path  $\mathbf{C}$ . When the index of refraction,  $n(\mathbf{r})$ , is a smooth function, the ray path  $\mathbf{C}$  satisfies the differential equation

$$\frac{d}{ds} \left( n(\mathbf{r}) \frac{d\mathbf{r}}{ds} \right) = \nabla n(\mathbf{r}) \quad (2.29)$$

where  $\mathbf{r}$  is the position vector of any point on the ray. For homogeneous medium ( $n = \text{const.}$ ), the ray path is represented by a straight line

$$\mathbf{r}(s) = \mathbf{a}s + \mathbf{b} \quad (2.30)$$

where  $\mathbf{a}$  and  $\mathbf{b}$  are constant vectors, and  $s$  is the ray path length.

### **2.2.1.1 Optical design and energy balance condition**

It is desirable to transform an input laser beam with Gaussian intensity profile into an output beam with uniform intensity profile while retaining the input wavefront shape. Further, it is often desirable to expand the laser beam diameter. To achieve these design goals, the optical surface shapes or index of refraction profiles may be used as design variables. Consider the geometrical configuration of a refracting laser beam profile shaping system shown in the Figure 2.8 [1]. The two curved surfaces

(reflecting or refracting, depending on the application) are used to satisfy the design conditions for shaping a laser beam profile.

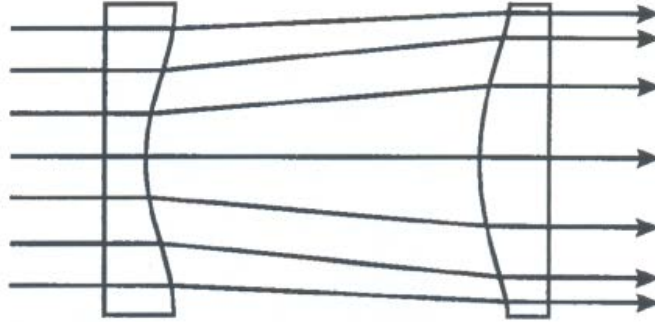


Figure 2.8 Ray paths in a conventional, refractive beam reshaping system.

Consider an incoming bundle of rays with an energy density  $\sigma(r)$  incident upon a lens system at a radial distance  $r$  from the optical axis. Then,

$$\sigma(r) = \exp\left[-2(r/r_0)^2\right] \quad (2.31)$$

where  $r_0$  is the radius of the beam. The conventional definition of the diameter of a laser beam waist is the location at which the field amplitude is  $1/e$  of its peak value. At the beam waist the beam intensity is  $1/e^2$  of its axial value. For a Gaussian beam, 86.5% of the total energy of the beam is contained within the waist. This beam leaves the optical system at a radial distance  $R$  from the optical axis with an energy density of  $\Sigma(R) = \text{const.}$

Integrating equation (2.23) over the incident and exit apertures gives

$$\int_0^{2\pi} d\theta \int_0^r \sigma(r) r dr = \int_0^{2\pi} d\theta \int_0^R \Sigma(R) R dR \quad (2.32)$$

where reflection and absorption losses have not been considered in equation (2.32). Since  $\Sigma(R)$  is a constant, the radius of beam in the exit  $R$  can be evaluated by carrying out the integration using equation (2.31) for  $\sigma(r)$  to obtain

$$R = \left\{ \frac{r_0^2}{2\Sigma} \left[ 1 - \exp(-2r^2/r_0^2) \right] \right\}^{1/2} \quad (2.33)$$

where

$$\Sigma = \frac{r_0^2}{2R_{max}^2} \left[ 1 - \exp\left(-\frac{2r_{max}^2}{r_0^2}\right) \right] \quad (2.34)$$

In equation (2.34),  $r_{max}$  is the working aperture of the first lens, and  $R_{max}$  is the corresponding point on the second lens.

Rays are refracted at surface  $s$  according to Snell's law, and the direction of refracted ray  $\mathbf{A}$  travelling from the point  $(r, z)$  on surface  $s$  to the point  $(R, Z)$  on surface  $S$  is given by equation (2.25) where the incident rays are along the optical axis, that is  $\mathbf{a} = \hat{\mathbf{k}}$ . Explicitly, a unit vector along the refracted rays over surface is given by

$$\mathbf{A} = \gamma \hat{\mathbf{k}} + \Omega \hat{\mathbf{n}} \quad (2.35)$$

where

$$\Omega = \frac{-\gamma + \{1 + (z')^2(1 - \gamma^2)\}^{1/2}}{[1 + (z')^2]^{1/2}} \quad (2.36)$$

$$\hat{\mathbf{n}} = (-z' \hat{\mathbf{r}} + \hat{\mathbf{k}}) / [1 + (z')^2]^{1/2} \quad (2.37)$$

$$\gamma = n/n_0 \quad (2.38)$$

$$z' = \frac{dz(r)}{dr} \quad (2.39)$$

The unit of vectors  $(\hat{\mathbf{r}}, \hat{\mathbf{k}})$  are along the  $r - z$  directions.

The ray path connecting  $(r, z)$  and  $(R, Z)$  is a straight line according to equation (2.30) with slope given by equation (2.35) and can be written as

$$(R - r)A_z = (Z - z)A_r \quad (2.40)$$

where  $A_r$  and  $A_z$  are the  $(r, z)$  components of  $\mathbf{A}$  given by equation (2.35). Combining equations (36) and (41) yields, after squaring and collecting terms in powers of  $z'$ :

$$\begin{aligned} & (z')^4[\gamma^2(R - r)^2 + (\gamma^2 - 1)(Z - z)^2] - (z')^3(R - r)(Z - z) \\ & - (z')^2(1 - \gamma^2)[(R - r)^2(Z - z)^2] - 2z'(R - r)(Z - z) - (R - r)^2 \\ & = 0 \quad (2.41) \end{aligned}$$

which can be factored and reduced to yield

$$\begin{aligned} & [(1 - \gamma^2)(Z - z)^2 - \gamma^2(R - r)^2](z')^2 + 2(R - r)(Z - z)z' + (R - r)^2 \\ & = 0 \quad (2.42) \end{aligned}$$

In equations (2.41) and (2.42),  $R$  is given by equation (2.33), and  $z$  is the solution to the differential equation, equation (2.42), as a function of the entrance aperture coordinate.  $Z$  in equations (2.41) and (2.42) is not known. For beam profile shaping intensity, the equation of the surface  $S$  expressed as  $Z = Z(R)$  will be adequate to solve the differential equation (2.42) for the shape of the surface  $s$ . For other beam profile shaping applications which seek also to control the shape of the output wavefront, the constant optical path length condition is used for rays passing through this optical system to determine the shape of surface  $S$ . The constant optical length condition yields a functional relationship between  $Z$  and  $z$  so that the differential equation (2.42) can be solved.

### ***2.2.1.2 Solution of the differential equations***

The goal of the optical design of a laser beam profile shaping system is define the optical components adequately so that the system can be analyzed, fabricated, and tested. This generally requires specification of the shapes of and spacing between the optical surfaces as well as the index of refraction of all the media. In contrast to conventional optical design, which optimizes the design parameters to minimize a merit function, the present method of solving differential equations defines the optical surfaces  $s$  and  $S$ . It does not seem possible to solve these differential equation analytically for  $z(r)$  and  $Z(R)$ .

Specifically, solving equation (2.42) as a quadratic equation for  $z'$  gives

$$z' = \frac{-(R - r)(Z - z) \pm n(R - r)\sqrt{(Z - z)^2 - (R - r)^2}}{(1 - n^2)(Z - z)^2 - n^2(R - r)^2} \quad (2.43)$$

where the positive solution for  $z'$  is used for the laser shaping lens configuration.

It is interesting to note that equation (2.42) permits  $z'$  to be expressed as a function of  $r$ , thus, enabling  $z(r)$  to be evaluated by an integration. Namely, the shape of the first element can be written as

$$z(r) = \int f(r)dr + C \quad (2.44)$$

where  $C$  is a constant, and  $f(r)$  is a known function. The shape of the second surface can be computed from the following expression:

$$Z(r) = z(r) + g(r) \quad (2.45)$$

where  $g(r)$  is another known function. The optical surfaces of both reflective and refracting laser profile shaping systems with collimated input and output beams satisfy equations in the form of equations (2.35) and (2.36).

### 2.2.2 Refractive intensity profile shaping systems

Laser beam profile shaping optics are well suited for applications whose overall efficiency increases when the irradiance over the detector is uniform, such as in a compact holographic projector systems. These compact holographic projection systems have been reported to offer a practical way to make a highly corrected mesh or grid pattern over curved surfaces where the pattern can range in size from sub-micron to multi-micron.

To understand this increase in system efficiency when using laser profile shaping optics, note that for a Gaussian beam with irradiance  $\sigma(r)$  given by equation (2.31), the intensity of the beam decrease to  $1/e^2 \cong 13.5\%$  of its axial value at the beam radius. The effect of this variation in beam intensity over a Gaussian beam is illustrated in Figure 2.9: (A) shows significant variation in pattern densities at the center and edge of beam for the same substrate and exposure time when laser profile shaping optics is not part of the system, and (B) shows almost uniform pattern densities at the center and edge of beam when laser profile shaping optics is part of the system.

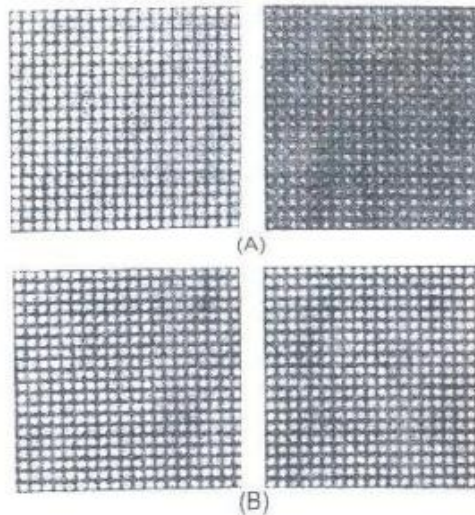


Figure 2.9 Interference pattern produced by a four-beam holographic projection processing system when illuminated with a Gaussian beam. The image on the left side of the figure was taken near the centre of the beam, and the image on the right side of the figure was taken near the edge of the beam.

Therefore, when beam shaping optics are introduced into a holographic projection processing system, as illustrated in Figure 2.10 the detector substrate will be uniformly illuminated, and photochemical reactions take place at the same rate over the entire substrate area, thus enabling the full beam diameter to be available for material processing. Introducing laser shaping optics into holographic projection processing systems have led to a significant increase in quality of micro-optics fabricated over the substrate.

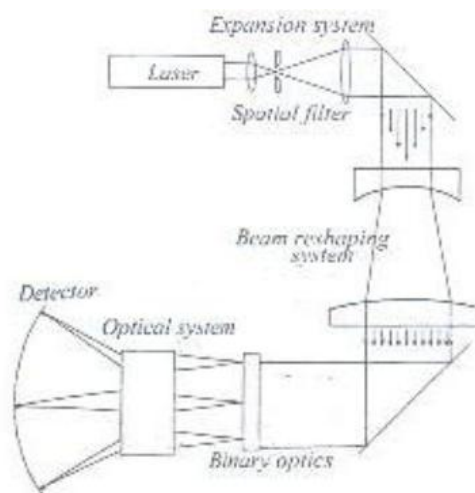


Figure 2.10 Holographic projection system

### **2.2.2.1 Method of design**

We are going to describe a refractive optical system for beam reshaping, which departs from earlier designs, to reduce as much as possible the difficult task of fabrication. An additional advantage of this design is that it is usable over a wide wavelength range, limited in practice by the bandwidth of the antireflection coating applied to the optics.

The most straightforward way to achieve uniform illumination with a Gaussian beam is to expand it to be much larger than area to be illuminated. One uses the central region of the beam, where the intensity varies slowly, and discards the rest. It is easy to see that this method of illumination is wasteful of laser light. If effective use of laser power is of no concern, this may be an acceptable solution, but often it is not.

To achieve uniform illumination while efficiently using laser power, one must transform the laser beam from the original Gaussian to a flattop (or top-hat) profile. Here we consider the more general problem of transforming a collimated Gaussian beam to a collimated, rotationally symmetric beam having some other radial profile. Although this task is more difficult, requiring careful attention to beam propagation, we believe it is worth the effort because the collimated beam can be adapted easily to applications that require different working distances and beam sizes, as well as to those that require uniform illumination of a volume rather than an area.

We apply the refractive approach, which is capable of high efficiency with a simple, coaxial optical arrangement, minimizing alignment issues. Our design procedure is straightforward, and the resulting surfaces, although aspheric, are rotationally symmetric and monotonic, which greatly reduces the difficulty of fabrication. Finally, use of low-dispersion material allows a single design to function well from ultraviolet to infrared wavelengths.

In the conventional design, Figure 2.8, one surface refracts the incident Gaussian beam to produce the desired flattop distribution at the second surface, which then recollimates the rays to generate a beam. The expansion is large for rays

that enter near the axis and smaller for rays entering near the edge, resulting in the desired modification of the intensity profile. The problem is that these systems neglect the boundary conditions at the edge of the beam. The design procedure is applied to that part of the Gaussian beam within some entrance aperture, typically containing the fraction  $1 - 1/e^2$  of the incident beam power, which is refracted in such a way as to generate an output beam of constant intensity while the rest of the beam is simply ignored. In practice an aperture intercepting  $1/e^2$  of the incident power will cause considerable diffraction into the output beam, leading to unwanted intensity variations. A complete solution to the beam reshaping problem must therefore take into account all the power in the incident Gaussian beam.

It is also essential to consider how the shape of the output beam affects its propagation. Any real laser beam has a finite diameter, hence a beam that is initially uniform over some aperture will eventually evolve to an Airy profile. Nevertheless, the flattop profile can be chosen so that within a substantial propagation range the effects of diffraction on the intensity distribution remain small.

We present a design that accepts essentially all (99.7%) of the input beam; generates a smoothly varying output beam for which diffraction effects can be controlled; and requires only monotonic, convex surfaces, which greatly simplifies the fabrication of the optics.

#### a. Definitions

We assume that the monochromatic (wavelength  $\lambda$ ) input and output beams are collimated and axially symmetric about the propagation direction, which we chose to be the  $z$  axis of a cylindrical coordinate system. The intensity of the input beam at radius  $r$  is given by the function  $f(r)$ , which is positive everywhere. The general intensity redistribution problem is to generate a beam with some other intensity distribution,  $g(r)$ , at the output of the optical system. We avoid apertures that would intercept appreciable optical intensity, therefore the total power for both the input

and the output beams must be the same. The intensity scale can be chosen so that the power is normalized:

$$2\pi \int_0^{\infty} f(r)r dr = 2\pi \int_0^{\infty} g(r)r dr = 1 \quad (2.46)$$

We also require that the radial intensity distribution be continuous. The input profile of greatest interest is the Gaussian profile:

$$f_R(r) = \left(\frac{2}{\pi w_0^2}\right) e^{-\left(\frac{2r^2}{w_0^2}\right)} \quad (2.47)$$

The requirements of normalization and continuity require  $g(r)$  to have a sigmoidal shape, approximately flat for small  $r$  and falling smoothly to 0 for large  $r$ . For such a distribution we require practical definitions of uniformity and efficiency because the intensity need not be exactly constant, the beam does not have a well defined edge, and all the input power is transferred to the output beam.

In general flattop beam is used to illuminate some object, or perhaps some cylindrical volume. If  $a$  denote the radius over which uniform illumination is required and  $g_{min}(a)$  and  $g_{max}(a)$  are the minimum and maximum values of  $g(r)$  within the region  $0 < r < a$ , then the relative peak to peak uniformity of the output beam over the aperture  $a$  is

$$U_{pp}(a) = \frac{g_{min}(a)}{g_{max}(a)} \quad (2.48)$$

Let us refer to the fraction of the total beam power that illuminates the region of interest as  $\eta(a)$ , the efficiency of utilization of the input beam.

$$\eta(a) = 2\pi \int_0^a g(r)r dr \quad (2.49)$$

Both  $U$  and  $\eta$  range from 0 to 1, with larger values being more desirable. They are not properties of  $g$  alone, but also depend on  $a$ . However, equations (2.48) and (2.49) implicitly define a relation between uniformity and efficiency that depend only on the beam shape.

## b. Choice of output beam profile

The lens design procedure can accommodate any output profile that satisfies the constraints of normalization and continuity, including piecewise or purely numerically defined functions. A good choice is the super-Gaussian distribution of order  $p$ :

$$g_{SG}(r) = g_0 e^{[-2(r/R_0)^p]} \quad (2.50)$$

with

$$g_0 = \frac{p 2^{2/p}}{2\pi R_0^2 \Gamma(2/p)} \quad (2.51)$$

$R_0$  serves as a length scale, and the shape is defined by the dimensionless order parameter  $p$ . The Gaussian profile is the special case  $p = 2$ , whereas for large  $p$  the profile is flat topped, as shown in Figure 2.11.

```
%% Super Gaussian profile %%  
  
R_0=1; % length scale (millimeters)  
p=[2 4 8 12]; % order  
r=-2:0.01:2; % x axis  
N=length(r);  
L=length(p);  
  
for i=1:L  
  
    for j=1:N  
  
        g_0=(p(i)*2^(2/p(i)))/(2*pi*R_0^2*gamma(2/p(i)));  
        g_SG(j)=g_0*exp(-2*(r(j)/R_0)^p(i)); % Super Gaussian  
distribution  
  
    end  
  
end
```

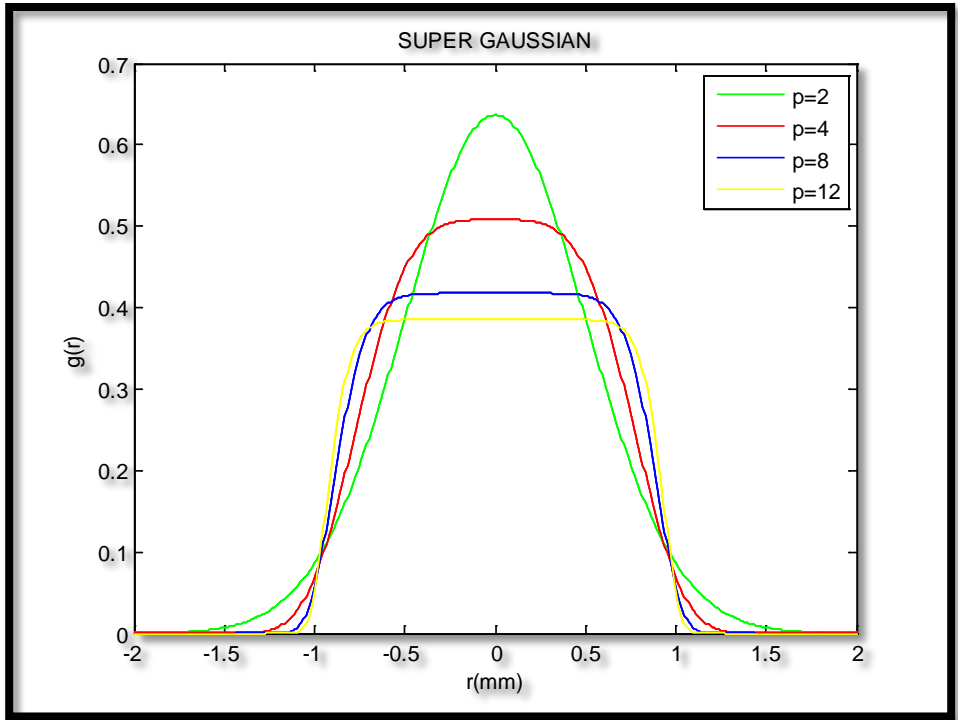


Figure 2.11 Super Gaussian function for  $p=2, 4, 8$  and  $12$ .

A Super Gaussian with large  $p$ , offers much greater efficiency than a Gaussian profile for a given level of uniformity. This is illustrated in Figure 2.12 [1], which shows how the peak to peak uniformity varies with efficiency for the Gaussian and several flattop profiles.

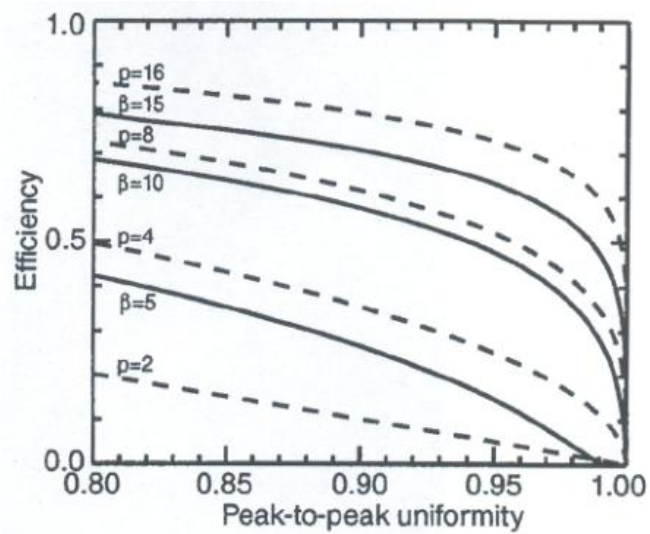


Figure 2.12 Relationship between efficiency and peak to peak uniformity for various beam profiles. Solid curves are for Fermi Dirac functions with, from bottom to top,  $\beta=5, 10$  and  $15$ ; dashed curves are for super Gaussian functions with, from bottom to top,  $p=2$  (Gaussian),  $4, 8$ , and  $16$ .

### c. Propagation

Because both uniformity and efficiency are desirable, it might seem advantageous to choose  $\beta$  or  $p$  as large as possible. However, aside from the practical issue of lens fabrication, diffraction places restrictions on the output profile. We set the task of generating a flattop beam, and in fact the only purpose of the second lens in Figure 2.8 is to collimate the output beam, to ensure that the field has constant phase across the output aperture. Let us suppose that an ideal optical system could perform this function perfectly and consider the evolution of the output beam. Assuming that the amplitude of the optical field at the output aperture  $u(r)$  is proportional to  $g^{\frac{1}{2}}(r)$ , and applying Kirchhoff's theory of diffraction together with the paraxial approximation, we obtain the following expression for the field at a radial distance  $x$  from the beam axis, after propagating through the distance  $D$  from the exit aperture:

$$u(x, D) \propto \int_0^a \rho U(\rho) J_0(k\rho x/D) e^{(ik\rho^2/2D)} d\rho \quad (2.52)$$

Here  $a$  denotes the exit pupil radius,  $k = 2\pi/\lambda$  is the wave number of the light,  $J_0$  is the Bessel function of order 0, and an overall phase and amplitude factor was omitted. Qualitatively, diffraction introduces ripples into the initially flat output profile, and for a given  $D$  the ripples are more pronounced the sharper the flattop profile is chosen to be. Quantitatively, for any  $D$  one can evaluate the uniformity versus efficiency of the diffracted beam by analogy to Figure 2.12. The numerical values for the desired uniformity and efficiency will, of course, be application dependent, but diffraction effects will appear in a similar manner for all applications. Whereas the relationship between uniformity and efficiency for  $g(r)$  depends only on the dimensionless shape parameter ( $\beta$  or  $p$ ), the range of propagation depends on  $R_0$  as well. This means that when diffraction effects are evaluated, the design must specify the beam size as well as its shape.

Figure 2.13 illustrates the effects of diffraction on two ideal Fermi Dirac profiles with  $R_0 = 3.25 \text{ mm}$ , one having a very abrupt edge,  $\beta = 150$ , and the other a more

gradual roll off,  $\beta = 16$ . The results would be the same if we use a Super Gaussian profile with different values of  $p$ . One can see that for  $\beta = 16$  the beam is virtually indistinguishable from the initial Fermi Dirac function, whereas for  $\beta = 150$  there are oscillations that are much larger than the nominal intensity. The range for which an efficiency of 50% is achieved with peak to peak uniformity of 90% is approximately 3 m for  $\beta = 16$  and only a few centimeters for  $\beta = 150$ .

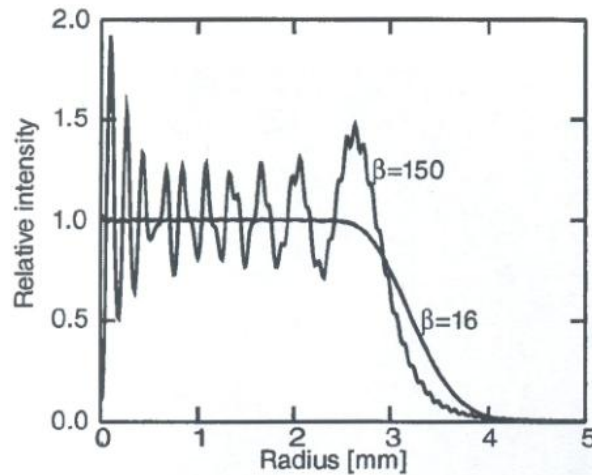


Figure 2.13 Effect of diffraction on Fermi Dirac beams with  $R_0 = 3.25 \text{ mm}$  after propagating  $1 \text{ m}$ .

#### d. Calculation of aspheric surfaces

The optical power of the lenses is not an important constraint, and the surfaces that we require are not steeply sloped. Of much more significance for practical fabrication is asphericity, the deviation of the required surface from the best fit spherical surface, and in this regard we find that designs with convex surfaces are comparable to those with a concave surface. It is also important that the Keplerian design always yields lens surfaces with a monotonic, convex form, which are considerably simpler to fabricate than the concave or even reentrant surfaces required by a Galilean design.

Figure 2.14 shows the schematic design of a Keplerian beam reshaper [1]. The first and last surfaces are shown as plane. The two lenses are assumed to have the same index of refraction  $n$ . We consider  $d$  like the distance between the points at

which the aspheric surfaces cross the  $z$  axis and introduce parallel coordinate axes  $\{r, z\}$  and  $\{R, Z\}$  centered on the intersections of the lens surfaces with the optical axis. The relation between the radii at which the ray enters and exits the optics,

$$R = h(r) \quad (2.53)$$

is referred to here as the ray tracing function. It is fundamental to the design of the optical system and directly related to the power redistribution problem. Energy conservation requires that the total power in the input beam enclosed by the ray that enters at  $r$  must be equal to the total power in the output beam enclosed by the ray that exists at  $R$ , resulting in an implicit equation for the ray tracing function,

$$\int_0^r f(x)xdx = \int_0^R g(x)xdx \quad (2.54)$$

which can be solved numerically for any given input and output intensity distributions. Because the beam energy enclosed in a circle of radius  $r$  must increase with  $r$ , it follows that the left and right hand sides of equation (2.54) are monotonic function of  $r$  and  $R$  respectively. Our normalization ensures that both functions range from 0 to  $1/2\pi$ .

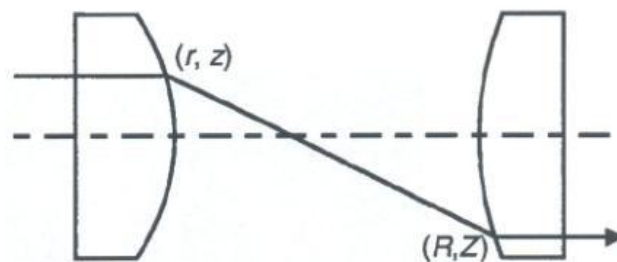


Figure 2.14 Schematic representation of a Keplerian beam reshaping system, showing the path of a typical ray.

The Galilean and Keplerian designs are distinguished by a formal sign difference in the ray tracing function, for  $r > 0$  the Galilean configuration has  $h(r) > 0$  whereas the Keplerian configuration is obtained when  $h(r) < 0$ .

The general ray shown in Figure 2.14 is defined by the four quantities  $r, z, R, Z$ . The ray tracing function relates  $r$  and  $R$ . The requirement that both the input and the output beams be collimated is equivalent to a requirement that the optical path difference from the input pupil to the output pupil be the same for all rays, which provides a second relation among these quantities. A third relation comes from Snell's law at the lens surfaces; the resulting system of equations exactly defines the two aspheric surfaces:

$$z(r) = \int_0^r \left\{ (n^2 - 1) + \left[ \frac{(n-1)d}{h(x) - x} \right]^2 \right\}^{-1/2} dx \quad (2.55a)$$

$$z(R) = \int_0^R \left\{ (n^2 - 1) + \left[ \frac{(n-1)d}{h^{-1}(x) - x} \right]^2 \right\}^{-1/2} dx \quad (2.55b)$$

Once the functions  $f$  and  $g$  are chosen, the only free parameters are the refractive index of the lenses and their separation. When we increase  $d$ , it reduces the asphericity of the lens surfaces.

Although the exact shapes of the aspheric lenses depend on the details of  $f$  and  $g$ , elementary geometric considerations lead to some general conclusions about the form of the Keplerian beam reshaping optics. In the Keplerian design all rays are deviated toward the optic axis, which implies that  $dz/dr$  has the same sign everywhere, which in turn means that the sag curve  $z(r)$  is monotonic. Hence, reentrant surfaces are impossible. Also, if the lens spacing is large compared to the dimensions of the lenses themselves, then the fact that  $h(x)$  is monotonic implies that the deviation of the ray at  $\{r, z\}$  increases monotonically with  $r$ . This means that the slope  $dz/dr$  varies monotonically from the center to the edge of the lens, and thus that the curvature of the lens surface has the same sign everywhere. In other words, the lens is locally convex everywhere, without any bumps or dimples. The same conclusions apply to the second lens, as one can see by tracing rays backward through the optics.

The constraint of the above paragraph do not apply to a Galilean design. In Figure 2.8, it is clear that the sign of the slope of the first lens at the radius  $r$  is the

same as the sign of  $h(r) - r$ . Although  $h(r)$  is required to be monotonic, there is no constraint on its magnitude. Hence  $h(r) - r$  can change sign across the surface of the lens, requiring a reentrant or wavy figure, depending on the details of the functions  $f$  and  $g$ .

## 2.3 Optimization techniques

Recently, the application of machine learning techniques including neural networks and genetic algorithms (GAs) to optimization problems has blossomed. Such techniques great promise not only because of their extraordinary efficiency and flexibility but also because they potentially allow the solution of previously intractable problems. So long as a multi-dimensional merit function can be well defined, a GA can be unleashed to roam this territory in an incessant search for the best solutions. The GA must no, however, be characterized as a mindless automaton that wanders aimlessly about this terrain. Indeed, the essence of its value lies in the fact the genetic algorithm yield computer-based complex adaptive systems that can evolve strategies that no human being ever devised.

Though there are numerous variations of GA's, they all share a central theme: their search strategy borrows concepts from natural selection and genetics. Once presented with a specific optimization problem, the GA produces a set of potential solutions. These solutions are referred to as "organism" and a set of organism is a "generation". GAs typically start with a randomly distributed seed generation,  $G(0)$ . For each generation  $G(t)$ , a new generation,  $G(t + 1)$  is produced based on the strengths and weakness of  $G(t)$ . These techniques attribute to Gas several unique features:

1. GAs work with a coding of the parameter set, not with the parameters themselves.
2. GAs search from a population of points, not a single point.
3. GAs use payoff, not derivatives or other auxiliary knowledge.
4. GAs use probabilistic transition rules, not deterministic rules.

This evokes the intriguing thought of employing GAs to find solutions to problems in optics and optical design where analytical methods are difficult to apply and other optimization techniques are extremely inefficient or fail to yield good solutions altogether. As a first step, one must develop a GA optimization method and apply it to several well-understood problems. The key to this "proof-of-principle" stage

lies in the fact that these problems have been attacked from a number of different perspectives.

The laser beam-shaping system problem can be solved by a number of different methods, some of which are numerical and some of which are analytical. Some may even employ a combination of both. Also, there are several classes of beam-shaping systems, the most popular being those using diffractive elements and those using refractive elements. Reflective systems have also been produced. The GA method can be used to optimize most systems of the above classes, which will be demonstrated by the solution of three profile-shaping problems.

For the first problem, the GA determines the shape of one surface of a beam-shaping element such that the wavefront of a beam entering the system is modified to have a uniform irradiance profile on a surface some distance away.

For the second problem, the GA is given two aspherical surfaces to shape, where each respective surface is part of a separate shaping element. The GA must do this with the constraints that the outgoing is parallel to the optical ( $Z$ -) axis and that it has a specified radius.

In the final problem, the GA not only must determine shaping attributes such as element thickness and surface shape, but also must choose gradient glass types from a catalog. Since the glass type can only be chosen from a finite set of values, the parameters that describe the glass types are discrete. Many conventional optimization techniques work in a continuous parameter space, since they are often driven by first and second derivatives. The ability to choose from discrete parameters is a particularly powerful feature of the GA, relative to other optimization codes.

### 2.3.1 Theory and Optimization

Generally, the idea behind optimization is that one has some function  $f$  which may be evaluated easily, usually computationally. This function is expressed in terms of several variables which may be discrete or continuous in nature. One wishes to find the values of these variables which make  $f$  assume either its maximum or minimum value. The difficulty of the problem is related to whether one is searching for local extrema, of which there may be many, or the global extrema, which represent the absolute best solutions. The complexity of the problem is related to the number of variables which make up  $f$ , in addition to ease with which  $f$  can be calculated. The greater the complexity of the problem, the longer it takes to arrive at a solution. Thus, search algorithms which arrive at solutions quickly are to be coveted.

Though there are myriad optimization techniques to choose from, methods such as GAs and simulated annealing are of particular interest because of their ability to solve combinatorial minimization problems. The key feature of such problems is that one or more of the parameters that make up the merit function (which is to be maximized) are discrete, in the sense that they can assume only particular values from a predefined set of allowable values. Thus, instead of an  $N$ -dimensional space made up of  $N$  continuous parameters, one is presented with a parameter space whose complexity is factorially large, so large in fact that it cannot be completely explored. It is here that GAs and simulated annealing techniques excel, though they also can be applied to problems that are purely continuous as well. It seems that of the three methods discussed here, no one method is necessarily more efficient than the others, though it does appear that GAs and the Tabu search tend to arrive at solutions more quickly than simulated annealing methods.

GAs produce a finite number of test solutions to a problem. Individually, these solutions are referred to as “organism” (or just “individuals”), and collectively as a “generation”. A generation is essentially an iteration. With each iteration, the merit function,  $M$ , is evaluated for each member of the generation. There may be as few as five or as many as hundreds of individuals per generation, depending on the code used

and how it is configured. An individual's genetic code represents a particular system prescription. For example, in the beam shaper projector, the six parameters that collectively define one surface of the beam shaping element are concatenated into a string. Thus, with each iteration, five or ten new system prescriptions are produced and their respective merit function evaluated.

### **2.3.2 Applications**

One key feature of the GA method is its broad applicability. One can adapt the GA to solve a multiplicity of problems. The problems presented below are chosen not only to demonstrate this advantage, but to do so while building a logical, concise method that scales from simple to more complex applications.

#### ***2.3.2.1 Design and Analysis of a Beam Shaper Projector***

The general goal here is to modify the shape of a lens element to uniformly illuminate a spherical surface some distance away. For this particular application, the use of a GA is perhaps a tad overzealous, considering that other more established design methods could be employed to produce solutions both easily and efficiently. The goal, however, is a long term one: the GA technique will be used to attack systems that are difficult to solve with more conventional methods. For example, certain holographic projection systems have fitness landscapes with 20 or more dimensions and extremely complex merit functions, making their solutions with conventional methods very tedious. For the short term, it must be established that the GA technique produces good solutions in a reasonably efficient manner. This is accomplished by the application of the GA technique to simple, well understood systems.

The application of a GA generally must satisfy two prerequisites. First, one must identify those parameters that fundamentally characterize the system. The parameters

must be numerically quantifiable and the modification of these parameters should have direct consequence on the system itself. Second, one must identify those features of a system which best describe the fitness (or “merit”) the system.

### ***2.3.2.2 Design and Analysis of a Gradient Index Shaper***

The beam shaper project problem presented in the previous section provides an example of a purely continuous merit function. Continuous merit functions can be solved by a number of different methods, and solving it with a GA is not particularly glamorous. As an example of more complex problem, the GA technique is used to design a gradient index shaper, which has a merit function that contain both continuous and discrete parameters.

### **3. Beam Integration**

The second, beam integration, includes methods where the input beam is broken up into components, which assemble at the target plane to produce the desired profile.

Integrators work for both coherent and multimode beams, where the input field distribution may not be known, and they are much less sensitive to alignment and beam size. However, interference effects are a problem with integrators, especially for coherent beams.

## **3.1 Beam shaping with diffractive diffusers**

We present an approach to beam shaping that often has a different realm of applications than the more conventional techniques. We discuss what is called a band limited diffuser. Many diffusers, such as ground glass, diffuse light over an angular volume that is often larger and not as well defined as desired. Diffractive diffusers offer a technique to diffuse light over a very well controlled angular spectral band.

To understand the properties of beam shaping with diffusers, it is useful to describe the difference between the other beam shaping techniques.

### **3.1.1 Properties of diffractive diffusers**

#### ***3.1.1.1 Near field beam shapers (remapping optics)***

Near field diffractive optics generally use a single diffractive order to produce the desired optical effect. In general, a diffractive optic such as a grating can use many diffractive orders. A simple example of a diffractive optic that uses only one diffractive order is a lens. Near field beam shapers are much like a complex aberrated lens that performs a remapping of the beam's energy distribution to provide the desired shape. The shaped beam will exist only at some predefined plane unless a second optic is used to correct the phase in the beam as shown in Figure 3.1. The resulting phase of a near field beam shaper can be canceled to produce a collimated beam which is allowed to diverge to give a shaped beam over an extended but finite range. The corrected shaped beam will experience diffraction and will degrade as the beam propagates. The diffraction of the corrected shaped beam will be as if the beam originated from an aperture function that is the same as the shaped beam. To minimize the diffraction of the edges, it is often advantageous to design the desired shape of the beam to have a soft or smooth edges. The function that is used to

describe the soft edge can have many forms. One such soft aperture function is a high order Gaussian or super Gaussian of the following form:

$$I \propto e^{2(r/w)^{2N}} \quad (3.1)$$

where  $I$  is the intensity,  $r$  is the radius,  $w$  is the waist radius and  $N$  is an integer. As the value of  $N$  increases, the closer the function approximates a true top hat function.

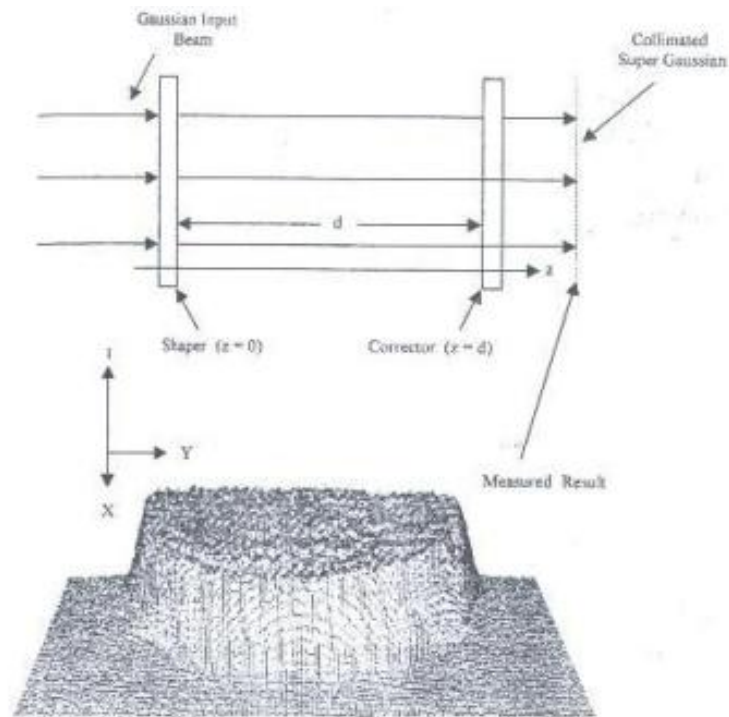


Figure 3.1 Typical system layout of a near field beam shaper. Only the first optic is required to shape the beam at plane  $z=d$ . To extend the range at which the top hat will exist requires a second optic to correct for aberrations in the phase of the beam.

It is possible to extend the range of a near field beam shaper by optically taking the Fourier transform of the output as shown in Figure 3.2. The lens transforms the shaped beam into its Fourier transform at the back focal plain of the lens. As the field propagates beyond the back focal plain, the diffraction caused by the propagation transforms the field back into the shaped beam with spherically diverging phase. This creates a diverging cone of light whose intensity envelope has the desired shape. Experimental results of this set up form a round super Gaussian are shown in Figure 9. The structure that is observed in the measured result is caused by multiple reflections within the system due to optics that do not have anti reflection coating. The beam can

then be collimated at any point by selecting the appropriate lens. This also allows one to size the output beam.

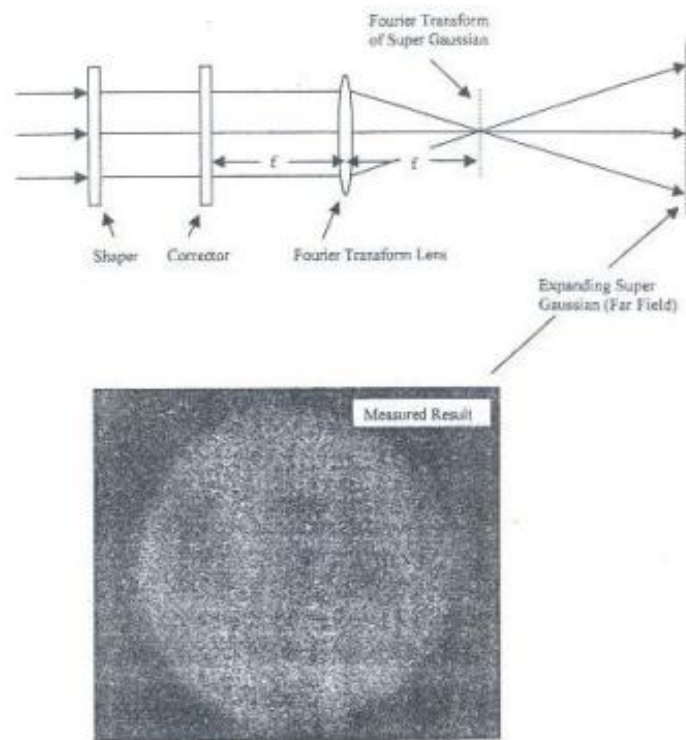


Figure 3.2 System to transfer the shaped beam into the far field. A simple lens with the appropriate focal length can be added after this system to re-collimate the beam.

Due to remapping nature of a near field beam shaper, the output is highly sensitive to the intensity and phase of the input beam. Any deviation in the input beam size, shape or location relative to the near field beam shaper will cause degradation to the resulting output. Figure 3.3 shows the output intensity of a simulation of a Gaussian to square top hat beam shaper [2]. There are several methods for designing the beam shaping diffractive optic.

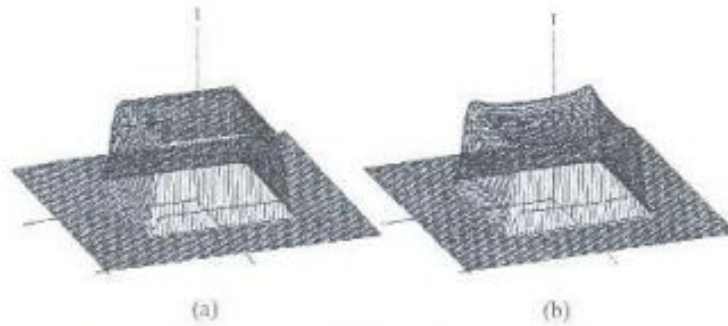


Figure 3.3 Simulations result of the output intensity of a Gaussian to square super Gaussian top hat beam shaper. (a) The result with the perfect input beam. The output is >99% efficient and the peak to valley non uniformity is <2%. (b) The result with an input that is 5% too large. The peak to peak non uniformity is about 18%.

From this, we see the sensitivity of the near field beam shaper to input beam variations. In general, the desired intensity footprint is maintained over a fairly large range of variations in input beams.

### 3.1.1.2 Far field shapers

Far field diffractive optics such as gratings and diffusers can in general use many diffractive orders in the case of gratings or spatial frequencies in the case of diffusers. Far field diffractive optics imparts a defined spatial frequency distribution to the phase of the laser beam. As the beam propagates, the spatial frequencies in the phase cause the beam to interfere with itself. Since the structure of such a device is made up of many very small phase apertures (typical < 10 wavelengths), the beam is in the far field almost immediately beyond the optic. This means that the resulting shape of the beam will continue to propagate with the predefined angular divergence as defined by the spatial frequencies in the phase. Figure 3.4 illustrates the extreme differences in the phase of a near field (single order) optic and a far field (multiple order) optic. On the left we can see the phase applied to the input field to generate the shaped beam shown in Figure 3.3. On the right we can see the phase of a diffuser that projects a square pattern.

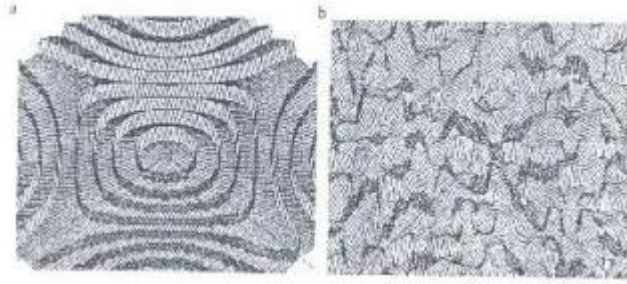


Figure 3.4 (a) The phase of the Gaussian to square super Gaussian top hat beam shaper shown in Figure 3.3. (b) A portion of the phase of a diffuser that projects a square energy envelope-

Far field optics have the advantage of being relatively insensitive to the shape, size, and alignment of the input beam. This is due to the multiplicative property of a Fourier transform. The resulting beam of a far field optic is simply the convolution of the Fourier transform of input beam and the spatial frequencies of the optic. The envelope of the output pattern is dominated by the phase function of the diffuser and not the shape of the input beam.

Gratings and diffusers are both far field diffractive optics and they share many characteristics. In general, a grating is a periodic amplitude and/or phase structure. To describe it we use the differential form of Maxwell's equations. This is the wave equation for the electric field:

$$\nabla^2 \mathbf{E} = \mu\epsilon \frac{\partial^2 \mathbf{E}}{\partial t^2} \quad (3.2)$$

where  $\mathbf{E}$  is the electric field vector,  $\mu$  and  $\epsilon$  are the material property parameters called the permeability and permittivity respectively.

Using Cartesian coordinates and choosing the scalar equation dependent on the  $z$  spatial coordinate we have

$$\frac{\partial^2 E}{\partial t^2} - \frac{1}{\mu\epsilon} \frac{\partial^2 E}{\partial z^2} = 0 \quad (3.3)$$

$$E(z, t) = Af_+(w_0t - k_0z) + Bf_-(w_0t - k_0z) \quad (3.4)$$

Equation (3.4) is the solution of the scalar equation (3.3) if

$$\frac{\omega_0}{k_0} \equiv \frac{1}{\sqrt{\mu\epsilon}} = v \quad (3.5)$$

where  $v$  is the velocity of the light in the medium. Equation (3.4) can be rewritten as

$$E(x, y, z, t) = Af(\omega_0 t - \mathbf{k}_0 \cdot \mathbf{r}) \quad (3.6)$$

Equation (3.6) is a wave with amplitude  $A$  and velocity  $v$  traveling in the  $\mathbf{k}_0$  direction.  $\mathbf{k}_0$  is called the propagation vector or the wave vector. The magnitude of the propagation vector is given by

$$|\mathbf{k}_0| = k_0 = \frac{\omega_0}{v} = \frac{2\pi}{\lambda} \quad (3.7)$$

where  $\lambda$  is the wavelength of the light in a given material and  $k_0$  is a constant while the light is propagating in the material. Figure 3.5 shows a circle whose radius is  $k_0$ . Along the  $k_x$  axis is a periodic structure with a grating vector of  $\mathbf{K}_g$  whose magnitude is given by

$$k_g = \frac{2\pi}{\Lambda} \quad (3.8)$$

where  $\Lambda$  is the period of the grating.  $\mathbf{K}_g$  has only an  $x$  component and adds to the  $x$  component of the propagating wave in discrete multiples. Due to the constraint that the wave vector has a constant magnitude of  $k_0$  we see that we can graphically determine the direction of the series of plane waves that result from the grating

$$\sin(\theta_t^m) = \frac{k_{0x} + mk_g}{k_0} \quad (3.9)$$

which then reduces to the familiar grating equation

$$\sin(\theta_t^m) = \sin(\theta_i) = \frac{m\lambda}{\Lambda} \quad (3.10)$$

where  $\theta_i$  is the incidence angle and  $\theta_t^m$  is the transmitted angle of a given diffracted order  $m$ . Orders (values of  $m$ ) that require  $|\sin \theta_t^m| > 1$  are called evanescent orders.

The wave vector of an evanescent order has an imaginary  $z$  component and thus attenuates exponentially beyond the surface of the grating.

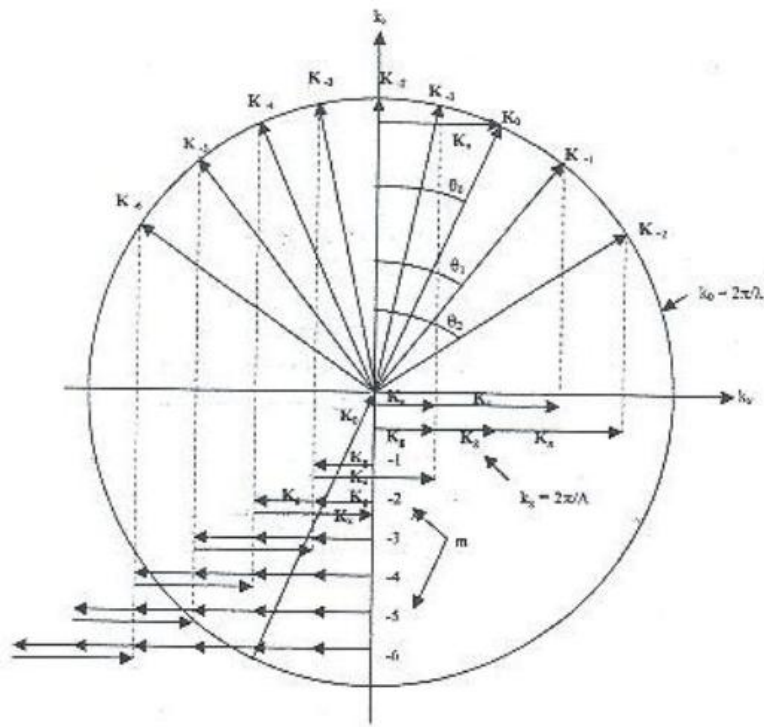


Figure 3.5 The wave vector map of light as it transmits through a periodically varying structure such as a grating. The lower portion of the plot shows the  $x$  component summations of the undeviated beam ( $K_0$ ) and the grating vector ( $K_g$ ).

### 3.1.1.3 Mathematical description of a diffuser

To mathematically describe a diffuser, we first note the shift property of the Fourier transform:

$$A(k_x - k_{x0}) \Leftrightarrow a(x)e^{-jk_{x0}x} = a(x)e^{-j\left(\frac{2\pi}{\Lambda}\right)x} \quad (3.11)$$

When designing optics such as diffusers, it is often useful to define things in term of a Discrete Fourier Transform. For a calculation grid of dimension  $D$ , the smallest frequency increment is  $\delta f = 1/D$ . Physically,  $D$  is the diameter of the input

beam or the period of a grating. Thus, any frequency is an integer multiple of  $\delta f$ . For example, define a frequency  $f_o$

$$f_o = N\delta f = \frac{N}{D} \quad (3.12)$$

or in terms of the wave number

$$k_{x0} = 2\pi f_o = 2\pi \frac{N}{D} \quad (3.13)$$

where  $N$  is an integer. From equations (48) and (3.4) it then follows that

$$\Lambda = \frac{N}{D} \quad (3.14)$$

Substituting equation (3.14) into equation (3.10), we find that any discrete spatial frequency can be described as

$$\sin \theta_t = \sin \theta_i + \frac{N\lambda}{D} \quad (3.15)$$

Recognizing the fact that  $D = \delta d(M - 1)$  where  $\delta d$  is the smallest distance increment and  $M$  is the number of data points across the calculation grid, we have

$$\sin \theta_t = \sin \theta_i + \frac{N\lambda}{\delta d(M - 1)} \quad (3.16)$$

Finally, solving the equation for  $N$  we have

$$N = [\sin \theta_t - \sin \theta_i] \frac{\delta d(M - 1)}{\lambda} \quad (3.17)$$

This equation is useful for computational reasons to calculate a particular grid point number on a discrete Fourier grid to produce a phase function of a given dimension that will bend light of a wavelength  $\lambda$  by an angle  $\theta_t$ .

### 3.1.2 Design example

Suppose we wish to design a binary diffuser with a clear aperture of  $D = 1.0 \text{ mm}$  that projects a ring of laser light with a wavelength of  $\lambda = 0.6328 \mu\text{m}$  between  $1^\circ$  and  $2^\circ$ . First we define the variables:

Name	Symbol	Value	Unit
Wavelegth	$\lambda$	$0.6328 \times 10^{-6}$	Meters
Aperture	$D$	0.001	Meters
Number of points	$M$	200	-
Transmitted angle	$\theta_t$	$1 < \theta_t < 2$	Degrees
Incidence angle	$\theta_i$	0	Degrees

Table 4 Definition of variables for the design of a diffuser

From equation (3.17)  $N_1 = N(\theta = 1^\circ) = 28$  and  $N_2 = N(\theta = 2^\circ) = 55$ . Notice that we have to round to the nearest integer. We now prepare a grid of 200 by 200 points with a width and height of 1.0 mm that is zero everywhere except grid points whose radius falls 28 and 55.

$$28 < R < 55$$

$$R = \sqrt{i^2 + j^2}$$

Where  $i$  and  $j$  are grid indices which have the range  $-100 < i, j < 99$ . Figure 3.6 shows the result.

```

%% Binary Diffuser

%% We define our system variables

D=0.001; % aperture (meters)
lambda=0.6328e-6; % wavelength (meters)
M=512; % points of the grid
theta_t=[1 2]; % transmitted angle
theta_i=0; % incidence angle

%% We calculate when the grid points are zero or have a height
of 1.00 mm

for i=1:2

    incr_d=D/(M-1);
    N(1,i)=round(((sin(theta_t(i))*2*pi/360))-
sin(theta_i*2*pi/360))*(incr_d*(M-1)/lambda));

end

for i=1:L

    for j=1:L

        r=sqrt(x(i)^2+y(j)^2);
        R=round(r);

        if(R>=N(1,1) && R<=N(1,2))
            Z1(i,j)=1;
        else
            Z1(i,j)=0;
        end

    end

end

mesh(x,y,Z1), colorbar

```

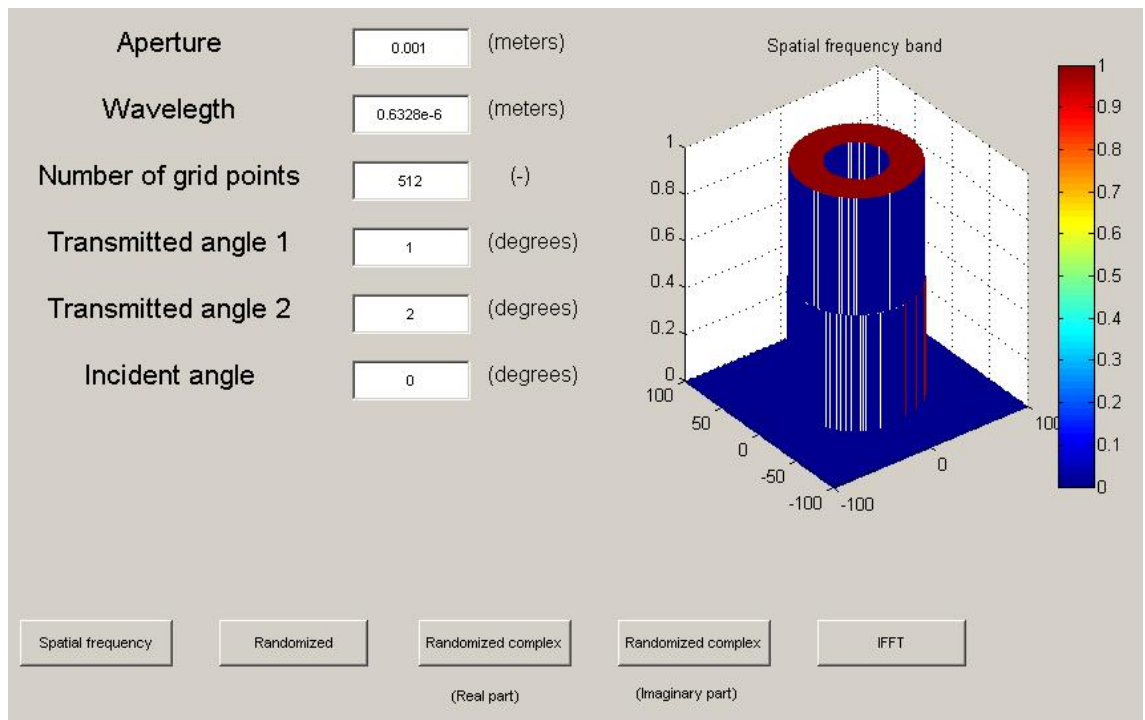


Figure 3.6 A plot of the spatial frequency band that is desired in the ring diffuser design example. The plot represents a subsection of the 200 x 200 calculation grid.

The next step is to randomize the non-zero values of the amplitude between 0 and 1 as we can see in Figure 3.7.

```
%% We randomize the grid
amplitude=rand(200,200);
Z2=Z1.*amplitude;
mesh(x,y,Z2), colorbar
```

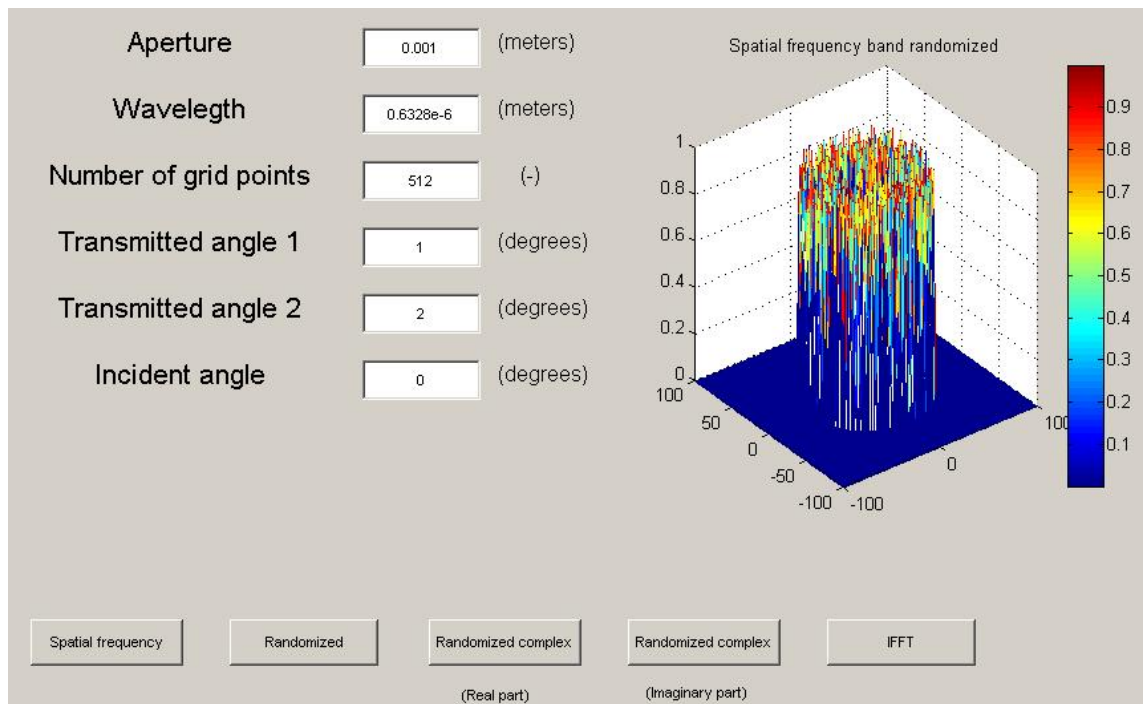


Figure 3.7 Randomized values between 0 and 1.

We must also randomize the phase between 0 and  $2\pi$ . The randomization step reduces the output dependence on the input beam. The high-frequency random function being multiplied by the desired frequency envelope insures that the spectral content of the envelope function is distributed over the full area of the binary diffuser. This removes any input beam alignment tolerances and any input beam intensity profile requirements. It is convenient at this point to insure that the complex grid is conjugated-symmetric, that is

$$f(i,j) = f^*(-i,-j) \quad (3.18)$$

In Figure 3.8 and Figure 3.9 we can see the real and the imaginary part of this complex grid.

```
% We randomize the phase and calculate the complex grid
phase=2*pi.*rand(200,200);
Z3=complex(Z2,phase);
mesh(x,y,real(Z3)), colorbar
mesh(x,y,imag(Z3)), colorbar
```

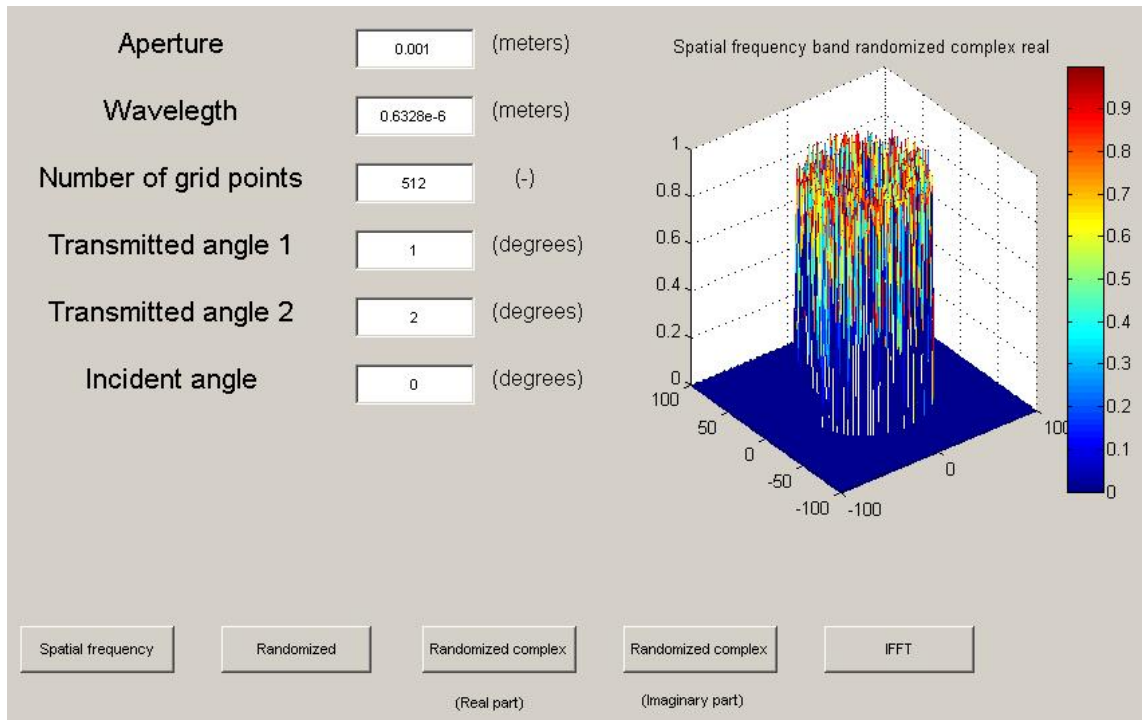


Figure 3.8 Spatial frequency band randomized real

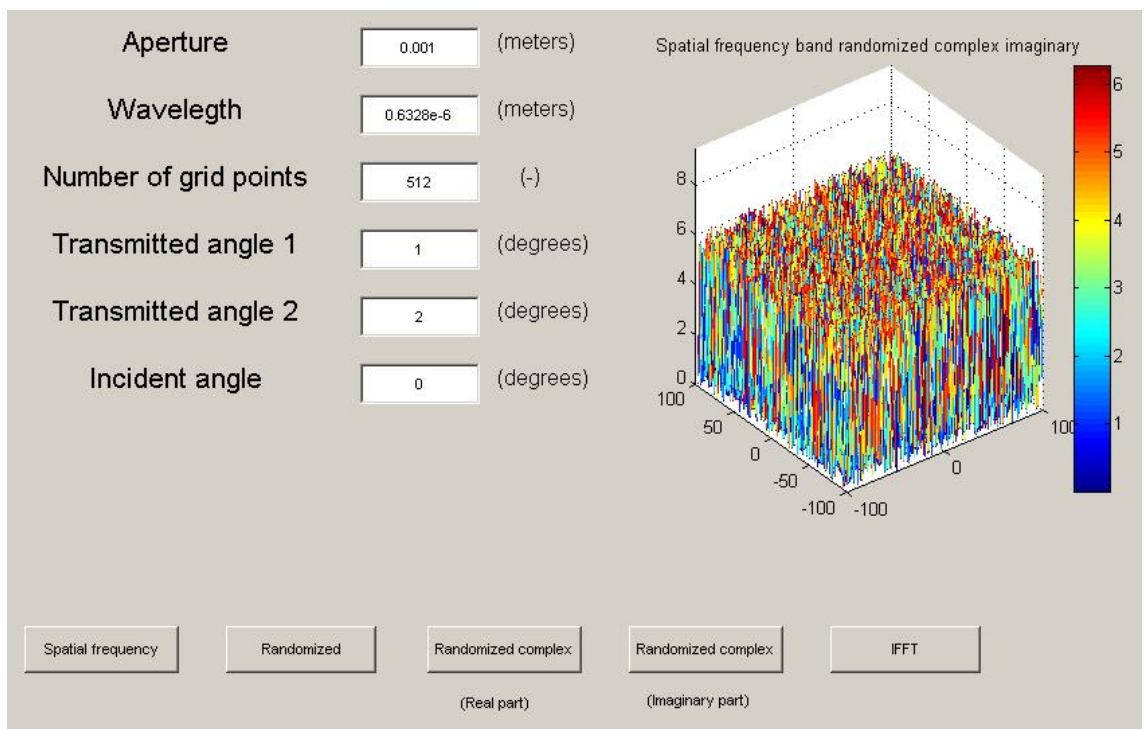


Figure 3.9 Spatial frequency band randomized imaginary

Then, the inverse FFT of the complex grid is calculated. Due to the conjugate-symmetry the result is real. All of the desired spatial frequency information is contained in the real part of the complex FFT. The real component of the grid is used as the phase for our optic, which contains the desired spatial frequency information. To reduce the phase to a binary diffractive optic, the phase is truncated to only two-phase levels, 0 and  $\pi$ . Assigning any positive value to  $\pi$  and any negative value to 0, will do this simply. Figure 3.10 shows the resulting phase profile. This example was for a symmetric pattern. For a non-symmetric pattern the conjugate-symmetric condition is not possible, which results in a complex field following the inverse Fourier transform.

```
%% We calculate the inverse FFT of the complex grid and reduce  
the phase to a binary diffractive optic.  
  
Z4=ifft2(Z3,'symmetric');  
  
for i=1:L  
    for j=1:L  
        if(Z4(i,j)>=0)  
            Z4_t(i,j)=pi;  
        else  
            Z4_t(i,j)=0;  
        end  
    end  
end  
  
mesh(x,y,Z4_t), colorbar
```

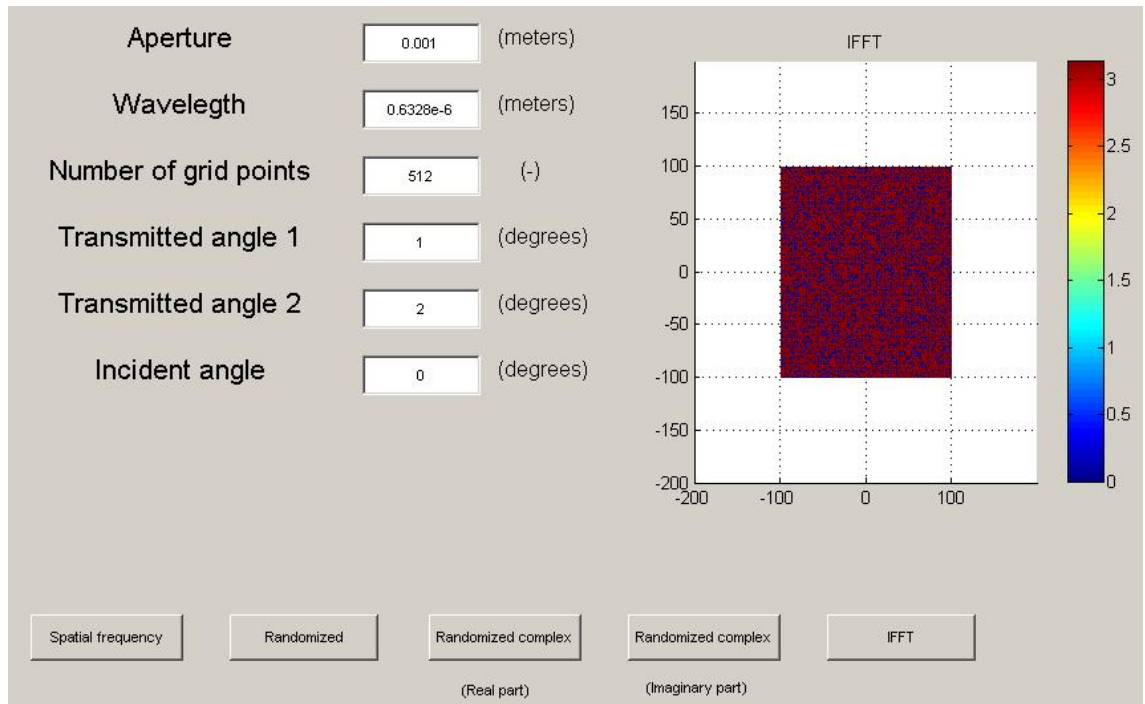


Figure 3.10 A portion of the binary (two levels) phase structure for the ring diffuser.

To verify our design we first assign an arbitrary amplitude function: Gaussian with  $w_0 = 0.25 \text{ mm}$ . We then simulate an optical Fourier transform by first applying a spherical phase to the field which simulates a lens of a given focal length and then propagating the field to the focal plane of the lens using a scalar theory code. Notice the high frequency content within the ring. This is the speckle characteristic of diffusers. Also notice the excellent suppression outside of the ring area. We know that at the focal plane  $r = f \tan(\theta)$  where  $r$  is the radius from the optical axis,  $f$  is the focal length of the lens and  $\theta$  is the angle of the incoming ray. From this, we can verify that the divergence angles of the design are indeed correct. These binary diffusers generally have an efficiency of about 70%.

### 3.1.3 Experimental results

In the previous text theoretical aspects of diffusers were introduced followed by practical realization if simulation. In this section the performance of the real optical system is compared with the ideal design. For this experiment we have used the ED1-C20 Engineered Diffuser with the next features [10]:

- Ø1" Diffusers
- Homogenize Input Illumination
- Circle Pattern Diffuser
- High Transmission Efficiency
- Achromatic Performance
- Unmounted
- Ideal for Low-Power Applications

Engineered Diffusers provide non-Gaussian intensity distributions in various patterns. This diffuser has a circle Tophat pattern with 90% transmission efficiency and a divergence of. Other diffusers, such as ground glass diffusers, cannot offer this advanced light control. His specifications are:

Pattern	Divergence	Transmission Efficiency
Circle	20° (Flat region)	0.9
	27° (50% - max)	
	36° (10% - max)	

Table 5 Specifications of the diffuser

As we can see in Figure 3.11 we have also used the next devices:

- Laser HeNe with a wavelength:  $\lambda = 632.8 \text{ nm}$ .
- Diffuser.
- Biconvex lens to collimate the ray.
- Set of two plano-convex lenses:
  1. Focal length:  $75 \text{ mm}$
  2. Focal length:  $25.4 \text{ mm}$



Figure 3.11 Realization of the experiment

Figure 3.12 show an image of the input beam. On the right side we can see the vertical and horizontal profile of the beam. Both of them have a Gaussian profile distribution as we said previously.

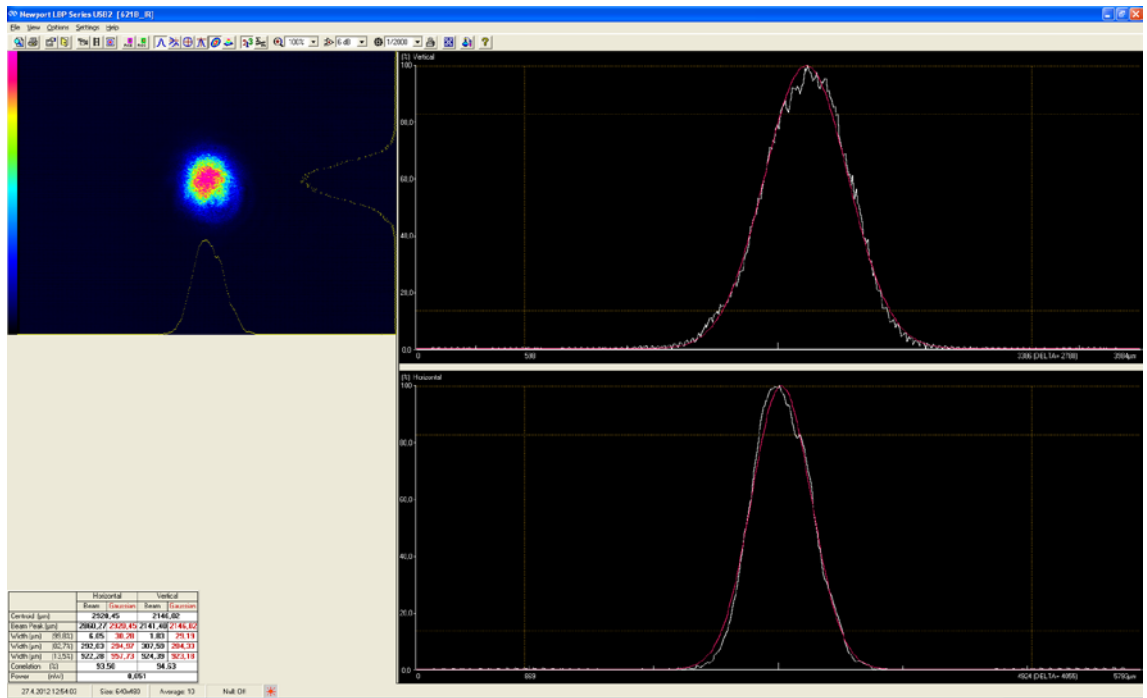


Figure 3.12 Input Beam

Figure 3.13 show the details of the diffuser. In the left side we can see as in Figure 3.10 a portion of the binary phase structure for the ring diffuser. In the right side we can see the profile of the diffuser, both vertical and horizontal. These profiles help the beam to transform in the output in a beam more uniform, a flattop beam. In Figure 3.14 we can see how have changed the beam. The profile is much more uniform than in Figure 3.12.

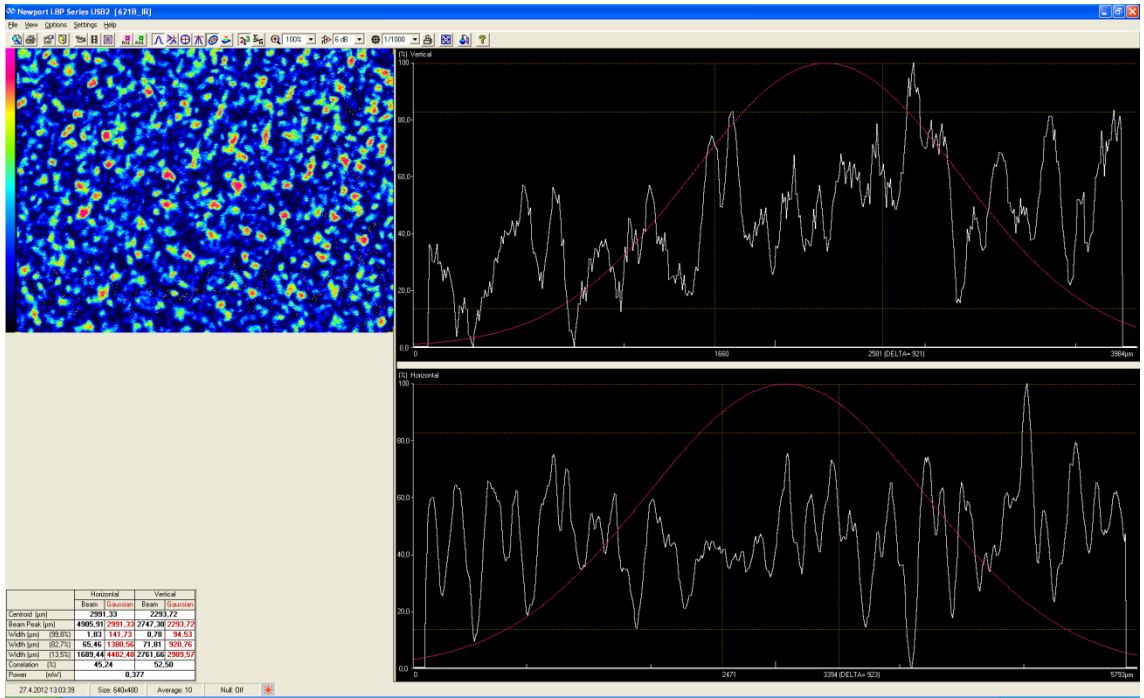


Figure 3.13 Diffuser detail

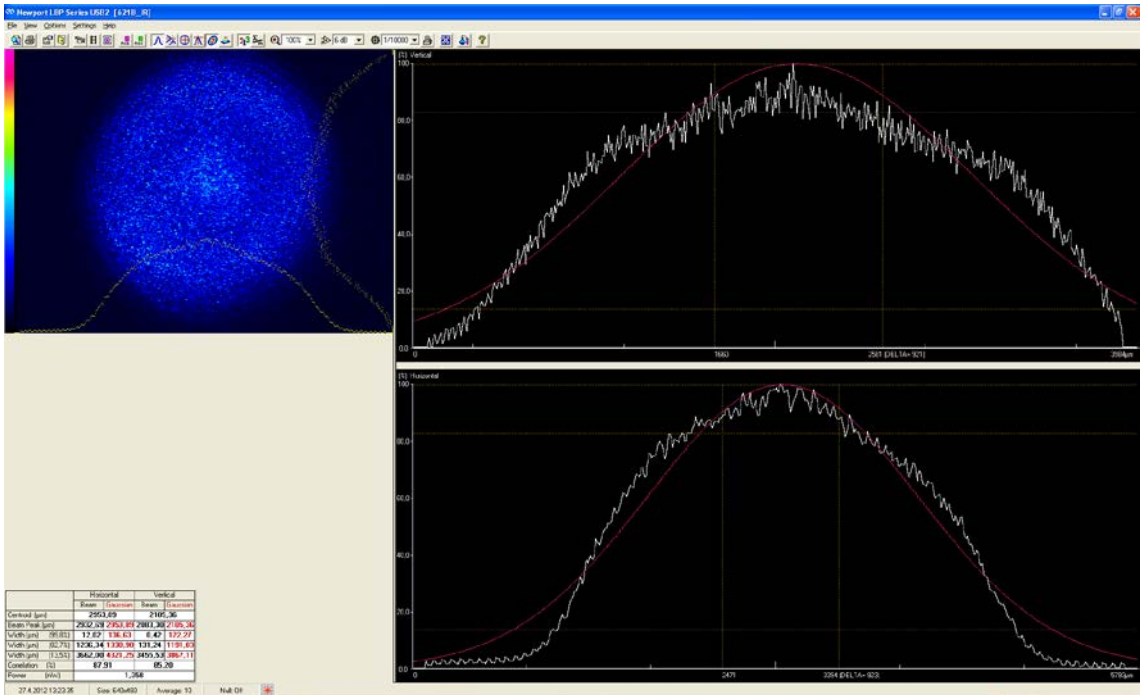


Figure 3.14 Output beam

### **3.1.4 Applications of diffusers**

The applications for diffuser beam shapers as opposed to near field beam shapers depend on the system limitation and the application requirements. Diffusers should be used in applications where the input beam quality and/or system alignment capabilities are not sufficient for a near field beam shaper. Factors that affect the input beam quality are the ability to measure the intensity and the phase of the beam, the stability of the beam with time, and the consistency of the beam from laser to laser. Near field beam shapers can only shape one mode of the laser. Diffusers will shape all modes of the laser and an increased amount of modes will lower the contrast of the speckle.

When designing a near field shaper for many different lasers, a series of measurements on many lasers must be taken to evaluate the variance of the input beams to determine if the variance in the resulting output is acceptable. It is prudent to design the optical system with a spatial filter and methods to adjust the beam to better match the designed input beam. Alignment to the beam shaper is critical. Depending on the specifics of the beam shaper, the errors in alignment often have a multiplicative effect on the errors observed in the output.

Diffusers should not be used in applications where the speckle is not acceptable and can not be reduced to a tolerable level. They are quite effective for high-power applications where the laser that is being used has a large number of mutually incoherent modes. They should also not be used when collimation of the shaped pattern is a requirement.

Diffusers are used to homogenize a light source, even a broad band light source. It should be noted that diffractive diffusers function with white light even though they are dispersive. They are used to illuminate a specific region for scanning applications. They are also used in alignment applications where a specific pattern is desired, such as laser targeting systems for firearms, machine tooling and assembly alignment systems, and even for space station to shuttle docking alignment. They can be used with illuminators for night vision systems, product marking systems, pen pointers with

corporate logos or sports team logos, laser light shows or increasing the viewing angle of a display. Diffusers could even be used in a wireless, free space inter-office communication network to reduce alignment requirements between components.

## 4. Conclusion

In the thesis was introduced several techniques or methods to solve the problem of laser beam shaping.

The first part deals with the description of the diffraction method. This part describes a diffraction theory based solution for the phase delay obtained using the method of stationary phase. The quality of the target spot was shown to depend on a parameter  $\beta$  that is a function of the input beam size, the target spot size, the focal length of the transform lens, and the wavelength.

The following part introduces geometrical methods. We have simulated a refractive optical system that transforms a Gaussian beam to a flattop beam. The essential points are use of positive lenses with convex, aspheric surfaces and the choice of an output power distribution that is properly normalized and continuous, with a radial roll off that minimizes diffraction effects.

The third part mentions other type of techniques based on optimization. This part demonstrates that genetic algorithms (GAs) methods can solve problems in optical design and theoretical optics. These optimization methods provide a means to produce solutions unfettered by convention or human influence.

In the final part, properties of diffractive diffusers are introduced. Furthermore, we have simulated an example of the ring diffuser and we have constructed an optical system with a laser, a diffuser, a biconvex lens and a set of two plano-convex lenses to verify the method. As we can see in the experiment, the difference between the input and the output profile is important due to the use of the diffuser so we can say that it is a good technique for high power applications which requires a uniform distribution in the system.

Other great technique, as we have already said, is geometrical method. The use of the aspheric lenses can reduce or eliminate spherical aberration and also reduce other optical aberrations compared to a simple lens. Therefore, output profile distribution will improve and the system we need construct will be much better.

## References

- [1] JOHN A. HOFFNAGLE AND C. MICHAEL JEFFERSON. Design and performance of a refractive optical system that converts a Gaussian to a flattop beam. *Applied optics Vol. 39, No. 30 y 20 October 2000.*
- [2] DICKEY, M. F., HOLSWADE, S. C. Laser beam shaping: theory and techniques. *New York: CRC Press, 2000.*
- [3] DICKEY, M. F., HOLSWADE, S. C., SHEALY, D. L. Laser Beam Shaping Applications. *New York: CRC Press, 2005.*
- [4] VLADIMIR OLIKER. Optical design of freeform two-mirror beam-shaping systems. *Vol. 24, No. 12/December 2007/J. Opt. Soc. Am. A.*
- [5] MERT SERKAN. Laser beam shaping optical system design methods and their application in edge-emitting semiconductor laser-based lidar systems. *December 17, 2007.*
- [6] BRIAN G. HENDERSON AND JUSTIN D. MANSELL. Laser Beam Shaping with Membrane Deformable Mirrors. *Active Optical Systems, LLC, 2021 Girard Ste 150, Albuquerque, NM 87106.*
- [7] DAVID L. SHEALY. Optical Design of Laser Beam Shaping Systems. *University of Alabama at Birmingham Tucson, 5 June 2002.*
- [8] ROBERT E. FISCHER, BILJANA TADIC-GALEB, PAUL R. YODER. Optical system design. *2008 The McGraw-Hill Companies, Inc; IND B F42A 11b.*
- [9] WARREN J. SMITH. Modern optical engineering: the design of optical systems. *2006; IND M F42A 37.*
- [10] <http://www.thorlabs.de/thorProduct.cfm?partNumber=ED1-C20>
- [11] [http://en.wikipedia.org/wiki/Aspheric\\_lens](http://en.wikipedia.org/wiki/Aspheric_lens)

## Appendix A

```
% Simulation of output beam

clear all
clc

% We define our system variables
a=[4.73974e-1 4.31128e-1;-5.50034e-2 -4.36550e-2;4.99298e-3
3.65204e-3;-2.37191e-4 -1.65025e-4;4.41478e-6 2.97368e-6];
xi=-(3*sqrt(2)):0.01:3*sqrt(2);
lambda=10.6e-3; %% millimeters
beta_x=8;
beta_y=16;
f=400; %% millimeters
y0=1; %% millimeters
n1=2.403;

% We initialize the vectors

N=length(xi);
phi1=zeros(N,1);
phi2=zeros(N,1);
x=[-2:0.01:2]; %% millimeters
y=[-4:0.02:4]; %% millimeters
L=length(x);
m=zeros(1,5);
n=zeros(1,5);
sagitta=zeros(1,L);

% We calculate the values of phi

for i=1:N

phi_1=a(1,1)*xi(i)^2+a(2,1)*xi(i)^4+a(3,1)*xi(i)^6+a(4,1)*xi(i)^8+a(5,1)*xi(i)^10;
    phi1(i)=phi_1;

phi_2=a(1,2)*xi(i)^2+a(2,2)*xi(i)^4+a(3,2)*xi(i)^6+a(4,2)*xi(i)^8+a(5,2)*xi(i)^10;
    phi2(i)=phi_2;
end

% We draw the rectangular and circular phase function

figure(1)
plot(xi,phi1,'g',xi,phi2,'r')
title('Phase function')
xlabel('Xi (normalized)')
ylabel('Phi (radians)')
legend('Rectangular','Circular')
grid on

% We calculate the radius for the incoming Gaussian beam
```

```

r0_x=(beta_x*f*lambda)/(2*sqrt(2*pi)*y0);
r0_y=(beta_y*f*lambda)/(2*sqrt(2*pi)*y0);
t=1;

%% We calculate the coefficients
for j=2:2:10

    m(t)=(a(t,1)*lambda*beta_x)*(sqrt(2)/r0_x)^j/(2*pi*(n1-1));
    n(t)=(a(t,1)*lambda*beta_y)*(sqrt(2)/r0_y)^j/(2*pi*(n1-1));
    t=t+1;
end

%% We calculate the sagitta of the phase surface
for k=1:L
    for p=1:L
        sagitta(k,p)=-
(m(1)*x(k)^2+n(1)*y(p)^2+m(2)*x(k)^4+n(1)*y(p)^4+m(3)*x(k)^6+n(3)
)*y(p)^6+m(4)*x(k)^8+n(4)*y(p)^8+m(5)*x(k)^10+n(5)*y(p)^10);
    end
end

%% We draw the output beam
figure(2)
mesh(x,y,sagitta), colorbar
title('Output beam')
xlabel('x(mm)')
ylabel('y(mm)')
zlabel('sagitta(mm)')

```

## Appendix B

```
%% Super Gaussian profile %%

clear all
clc

R_0=1; % length scale (millimeters)
p=[2 4 8 12]; % order
r=-2:0.01:2; % x axis
N=length(r);
L=length(p);
g_SG=zeros(1,N);
color=['g' 'r' 'b' 'y'];

for i=1:L

    for j=1:N

        g_0=(p(i)*2^(2/p(i)))/(2*pi*R_0^2*gamma(2/p(i)));
        g_SG(j)=g_0*exp(-2*(r(j)/R_0)^p(i)); % Super Gaussian
distribution

    end

    plot(r,g_SG,color(i))
    title('SUPER GAUSSIAN')
    xlabel('r(mm)')
    ylabel('g(r)')
    legend('p=2','p=4','p=8','p=12')
    hold on

end
hold off
```

## Appendix C

```
%% Binary Diffuser

clear all
clc

%% We define our system variables

D=0.001; % aperture (meters)
lambda=0.6328e-6; % wavelength (meters)
M=512; % points of the grid
theta_t=[1 2]; % transmitted angle
theta_i=0; % incidence angle

%% We initialize the vectors

N=zeros(1,2);
x=[-100:1:99];
y=[-100:1:99];
L=length(x);
Z1=zeros(1,L);

%% We calculate when the grid points are zero or have a height
of 1.00 mm

for i=1:2

    incr_d=D/(M-1);
    N(1,i)=round(((sin(theta_t(i))*2*pi/360))-
sin(theta_i*2*pi/360))*(incr_d*(M-1)/lambda));

end

for i=1:L

    for j=1:L

        r=sqrt(x(i)^2+y(j)^2);
        R=round(r);

        if(R>=N(1,1) && R<=N(1,2))
            Z1(i,j)=1;
        else
            Z1(i,j)=0;
        end

    end

end

%% We draw the graph

mesh(x,y,Z1), colorbar
```

```

title('Spatial frequency band')
axis([-100 100 -100 100 0 1])
rotate3d

%% We randomize the grid

amplitude=rand(200,200);
Z2=Z1.*amplitude;
figure(2)
mesh(x,y,Z2), colorbar
title('Spatial frequency band randomized')
axis([-100 100 -100 100 0 1])
rotate3d

%% We randomize the phase and calculate the complex grid

phase=2*pi.*rand(200,200);
Z3=complex(Z2,phase);
figure(3)
mesh(x,y,real(Z3)), colorbar
title('Spatial frequency band randomized complex real')
axis([-100 100 -100 100 0 1])
rotate3d

figure(4)
mesh(x,y,imag(Z3)), colorbar
title('Spatial frequency band randomized complex imaginary')
axis([-100 100 -100 100 0 3*pi])
rotate3d

%% We calculate the inverse FFT of the complex grid and reduce
the phase to a binary diffractive optic.

Z4=ifft2(Z3,'symmetric');
Z4_t=zeros(L,L);

for i=1:L
    for j=1:L
        if(Z4(i,j)>=0)
            Z4_t(i,j)=pi;
        else
            Z4_t(i,j)=0;
        end
    end
end

figure(5)
mesh(x,y,Z4_t), colorbar
title('IFFT')
axis([-200 199 -200 199])

```